Brain Multiphysics 3 (2022) 100058

Contents lists available at ScienceDirect

Brain Multiphysics

journal homepage: www.sciencedirect.com/journal/brain-multiphysics

Multiscale co-simulation of deep brain stimulation with brain networks in neurodegenerative disorders

Hina Shaheen *, Swadesh Pal, Roderick Melnik

MS2 Discovery Interdisciplinary Research Institute, Wilfrid Laurier University, Waterloo, Canada

ARTICLE INFO

Keywords:
Deep brain stimulation
Brain connectome
Parkinson's disease
Basal ganglia
Laplacian operator
Neurodegenerative disorders
Multiscale modeling

ABSTRACT

Deep brain stimulation (DBS) has been used successfully as symptomatic treatment in several neurodegenerative disorders, including Parkinson's disease (PD). However, the mechanisms of its activity inside the brain network are unclear. Many virtual DBS models investigate the dynamics of a subnetwork surrounding the basal ganglia (BG) as a spiking network has been attracting a growing body of research in neuroscience. Connectomic data, on the other hand, show that DBS has a wide range of impacts on many distinct cortical and subcortical sites. Notably, the nonlinear reaction–diffusion multiscale mathematical models demonstrate the effectiveness of capturing crucial disease characteristics and are used to simulate large-scale brain activity. The BG and associated nuclei comprise many subcortical cell groups in the brain, and their couplings commonly revealed MRI-based assessments of the strength of anatomical connections. We have developed a hybrid modeling formalism and a unique co-simulation technique that allows us to compute electrodiffusive ion dynamics for the cortex–BG–thalamus (BGTH) brain network model within a large-scale brain connectome. We collect data from the Human Connectome Project (HCP) and propose a closed-loop DBS approach based on the brain network model. Moreover, we select regions in the parameter space that reflect the healthy and Parkinsonian states as well as the impact of DBS on the subthalamic nucleus (STN) and globus pallidus internus (GPi) neurons. We predicted that if we apply the DBS to the system described by the temporal model, the brain maintains a healthy state until 0.05ms for STN neurons and 0.035ms for GPi neurons. A local regulatory mechanism known as feedback inhibition control (FIC) points to the existence of underlying network dynamics in the white matter of connected brain regions. The model showed unanticipated effects that in the presence of diffusion, the human brain maintained a healthy state for a long time after the DBS had been applied to STN and GPi neurons. This research helps us better understand the changes in brain activity caused by DBS and enhances this clinical therapy, thus shedding new light on the importance of DBS mechanisms in BGTH brain network models of neurodegenerative disorders.

1. Introduction

Deep brain stimulation (DBS) is a procedure that uses high-frequency electrical stimulation delivered by electrodes implanted in the brain to treat a variety of movement disorders, including Parkinson's disease. It has been suggested that the overall effect of DBS is to block neuronal activity in the stimulated region [1]. However, its mechanisms of action inside the brain networks remain unknown. The most substantial DBS research has been conducted in movement disorders, which share the pathophysiology of connections between the basal ganglia (BG), thalamus (TH), and cortex [2–4].

The basal ganglia, along with the thalamus (BGTH) and cortex, form a complex network of nuclei composed of several subcortical cell groups involved largely in motor control, as well as a broader range of activities including motor learning, executive processes, behavior, and emotions [5,6]. The term basal ganglia refer to deep nuclei inside the brain hemispheres (striatum or caudate-putamen and globus pallidus), although related nuclei include structures in the diencephalon (subthalamic nucleus), mesencephalon (substantia nigra), and pons (pedunculopontine nucleus). The theory that PD patients have a lower level of activity in the thalamic region, which causes a motor function to be compromised and results in bradykinesia or akinesia, has a long history [7]. Clinical observations in the 21st century profoundly changed ideas and beliefs about the activities of the basal ganglia. They demonstrated that lesions of the lenticular nucleus (putamen and globus pallidus) and the subthalamic nucleus (STN) are linked to PD [8]. The striatal inhibitory circuits are important for motor function, and the unbalanced activity of striatal medium spiny neurons is thought

* Corresponding author.
E-mail addresses: shah8322@mylaurier.ca (H. Shaheen), spal@wlu.ca (S. Pal), rmelnik@wlu.ca (R. Melnik).

https://doi.org/10.1016/j.brain.2022.100058
Received 30 May 2022; Received in revised form 21 October 2022; Accepted 3 November 2022
Available online 11 November 2022

to be the cause of altered firing in the globus pallidus (GP) [6,9]. The GPi and STN are clinically most important stimulation targets for PD [3,10–12]. It is a typical strategy to model the neurons in these important areas for DBS as a network, using mathematical descriptions of neuronal functions and connections [12–14].

Previous research has made significant advances in developing Parkinsonian network dynamics models that assume differences between PD and healthy patients in terms of functional connection strengths or striatal projection neuron activity levels [15,16]. Many virtual DBS models have been studied on a subnetwork around the basal ganglia and its dynamics as a spiking network, with experimental evidence validating their features [17,18]. The Rubin–Terman model [19] was one of the spiking neuronal models of the BGTH network used to simulate DBS. This model employs Hodgkin–Huxley (HH) neurons to reproduce the four key cell types in the BGTH: STN, GPi, GPe (globus pallidus externus), and TH neurons, which are all connected by simulated synaptic connections in the extracellular space (ECS) of the brain. Computational models are required to build closed-loop control techniques because they help to understand how the system reacts to stimuli and give insights into membrane potential activation. Analyses of membrane potentials of ions in the brain's ECS are considered to be a marker of neuronal signaling [20]. Classifying the distribution of carefully chosen membrane potential in different brain regions can provide structural information about the human brain connectome. The fundamental idea is that diffusing ions conduct random walks to examine the different regions of the large-scale brain network [21]. Therefore, it makes biological sense to include ion diffusion on the spatio-temporal scale of the brain. In order to predict how these potentials will be distributed, it is necessary to understand the effective ion diffusion coefficients in different brain regions. Diffusion analysis offers a novel view into a field that has previously been mostly inaccessible through experiments [22,23]. Importantly, deviations from ideal diffusion behavior can be used to investigate the biological activity of individual neurons [22,24–26]. Diffusion in the ECS requires a deep dive into neuronal cell biology for a variety of reasons. One is to provide sustained electrical signaling in the central nervous system (CNS) by supplying a reservoir of extracellular ions to individual neurons, adequate to maintain resting, synaptic, and action potentials [23,27]. In the CNS, diffusion is generally uneven and non-uniform (anisotropic). Neurons communicate with one another via synapses and the diffusion of substances that are neuroactive in the ECS. Moreover, glial cells do not have synapses and can only communicate with neurons through the diffusion of ions and neuroactive substances in the ECS. Indeed, the interaction of a neuron with glial cells at a specific synapse must involve the diffusion of a transmitter and ions produced by the neuron to the synaptic cleft via the underlying ECS [22,28]. Using extracellular electrodes to monitor membrane potentials is one of the most commonly used experimental techniques for examining brain activity [29–31]. The relationship between the ECS potentials and the underlying neural processes is frequently investigated using computer simulations [32,33].

Moreover, recent multiscale mathematical modeling works have demonstrated the utility of nonlinear reaction–diffusion type equations in identifying neuropathology [34–36]. Importantly, connectomic data reveals that DBS has extensive effects on many different cortical and subcortical locations [37]. Discrete brain network models in a spatio-temporal domain construct the dynamics of model parameters that are used to simulate large-scale brain activity [38–40]. The strengths of anatomical connections based on diffusion tensor imaging (DTI) data mediate system connectivity (structural connectivity or connectomes) [38]. In biological objects, DTI truly appears as a diffusion constraint, and it is sensitive to pathological changes in these mechanisms [41]. These pathological changes have a considerable influence on the magnetic resonance imaging (MRI) signal, which is essential for the early diagnosis of brain injury. [42,43]. We have created a hybrid modeling formalism in the current study that enables us to compute the electro-diffusive ion dynamics in the ECS around activated neurons. It is noteworthy that none of the previous computational studies have revealed that diffusion can be involved in brain network dynamics when it is known that the ions diffuse from one brain region to another [12, 23,27,44]. This gap might have occurred because human studies using diffusion techniques to assess anatomic connectivity (i.e., DTI) give incomplete information about the connectivity between regions supported by local association fibers and neighborhood association fibers that link nearby and adjacent regions [45,46]. Most diffusion imaging techniques either discard fibers or insufficiently measure information from nearby or adjacent regions [47–49].

To cover this knowledge gap, in this paper, we implement a novel co-simulation approach of a modified Rubin–Terman model for subcortical brain regions in and around the basal ganglia on the whole cerebral hemisphere. We interface this novel approach with a discrete brain network model for each cortical region including ion diffusion on the large-brain scale to better fit experimental data on neuron firing characteristics. Following [34], our basic strategy is also to investigate some of the essential aspects of the dynamics of the model, e.g., the influence of DBS on both healthy and diseased states. We show that the eigendecomposition of the Laplace operator having ion diffusion can predict the collective dynamics of human brain activity at the macroscopic scale [34,50]. The network model is made up of linked spiking neurons in the ECS that are based on biophysical principles, and the PD state is defined by a thalamic relay reliability distortion. Finally, we found regions in the parameter space demonstrating the healthy and Parkinsonian states and examined the transition from a healthy state to a pathological state and the impact of DBS on subcortical regions in and around the basal ganglia. We collected the data from the Human Connectome Project (https://braingraph.org) to find the diffusion tensor in the brain network model. Our model can capture a real scenario, as we considered real brain connectome data. This work focuses on computational modeling of the membrane potentials in the cortex–BGTH regions in the spatio-temporal domain of the human brain which helps experimentalists with some early observations of these potentials [51,52]. The results obtained allow us to better understand the changes in brain activity induced by diffusion and the effect of DBS on brain networks, and to clarify how these complex systems are assembled during development and undermined by disease, particularly in targeting neurodegenerative syndromes and neural activity.

The rest of the paper is organized as follows. In Section 2, we describe our model in its different components: (i) a discrete brain network model of the BGTH brain network; (ii) a continuous model of the BGTH brain network; and (iii) DBS dynamics. In Section 3, we present numerical simulations based on the developed discrete brain network models for the cortex–thalamus–basal-ganglia system and discuss our results. The computational results have been done in C-language and SHARCNET supercomputer facilities provided by Ontario, and the simulation results have been plotted in MATLAB. Finally, we conclude our findings and outline future directions in Section 5.

2. Mathematical modeling of deep brain stimulation in brain network

In this section, we present the: (a) continuous model of the BGTH network mediated by diffusion terms, and (b) discrete brain network model of the BGTH system, giving particular attention to Laplacian terms. We evaluated the behavior of each specific kind of neuron in the ECS in the brain region and patterns of firing under healthy and pathological states to validate the features of the BGTH model. Subsequently, we analyze the firing rates of the interconnected neurons on each node in the brain network with data. Finally, the effects of DBS on GPi, and STN in the putamen, globus pallidus and thalamus are then compared to previous results of the effects of DBS frequency on symptoms.

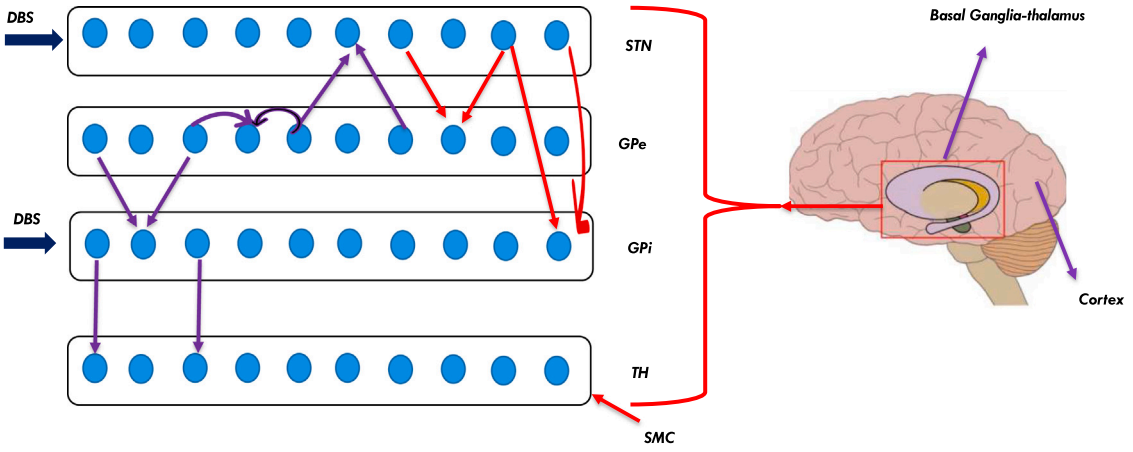

Fig. 1. The cortex–BGTH network model. The nuclei's connections are based on established physiology, the red arrows indicate the excitatory projections, and the purple arrows represent the inhibitory connections [12]. The SMC denotes the excitatory input from the SMC to the TH. Blue arrows indicate the DBS input to the STN and GPi. (For interpretation of the references to color in this figure legend, the reader is referred to the web version of this article.)

2.1. Continuous model of cortex-BGTH network

In the present section, we introduce the diffusion terms in the mathematical model of the BGTH system. The continuous BGTH network model used here was proposed by Lu et al. [12]. It was modified from the traditional Rubin–Terman model [19] to better fit experimental data on neuron firing characteristics and is used to investigate the impact of neuronal activation or silencing on information relay through the TH. This BGTH network model is made up of four major nuclei: STN, GPi, GPe, and TH, which are coupled by numerous excitatory and inhibitory synaptic connections which react to information from the sensorimotor cortex(SMC). This is the main reason behind mentioning the cortex with the BGTH system, as the SMC signal comes from the cortex. Each STN neuron in this sparsely linked network gets inhibitory inputs from two GPe neurons, as illustrated in Fig. 1. Each GPe neuron is stimulated by two STN neurons and inhibited by two additional GPe neurons. In addition to excitatory inputs from two STN neurons, each GPi neuron gets inhibitory inputs from two GPe neurons. Finally, a single GPi neuron provides inhibitory input to each TH neuron, whereas the SMC provides an excitatory input. The striatal input is represented by a constant current supplied to GPe neurons. This algorithm has been first proposed in [19], and then modified in several studies [12,53]. The temporal dynamics of the BGTH network mathematical model is adopted from [12], where the neurons of STN, GPe and GPi are modeled by the same set of HH type of equations, and their differences are in parameter settings and modifications in neuron-specific currents as given in Table 1. Note that there are some typos in [12] in the parameter settings and neuron-specific currents, which have been corrected in our Table 1. We are interested in the interaction between different brain regions involved in the BGTH network motivated by healthy and pathological states in the brain observed in PD. This is due to the heterogeneous distribution of the ions present at the time scales typical for the whole brain. Such ions diffuse between nodes (brain regions) to maintain ionic homeostasis. Towards this end, we set up a reaction–diffusion model for STN, GPe, GPi, and TH. Before going to the discrete brain network model, we first consider a continuous, non-linear reaction–diffusion equation in a bounded domain $\Omega \subset \mathbb{R}^3$ (domain of interest) for four brain nuclei. For $x \in \Omega$ and time $t \in \mathbb{R}^+$, let $v^p = v^p(x,t)$ be the membrane potential of STN ($p = sn$), GPe ($p = ge$), GPi ($p = gi$), and TH ($p = th$) neurons in the putamen, globus pallidus and thalamus, brain regions. Then, the development of membrane potential is regulated by:

$$\frac{\partial v^{sn}}{\partial t} = \frac{1}{c_m}\left(-I^{sn}_{Na} - I^{sn}_{K} - I^{sn}_{L} - I^{sn}_{T} - I^{sn}_{Ca} - I^{sn}_{ahp} - I_{ge\to sn} + I_{snapp}\right) + \nabla\cdot(D_{v^{sn}}\nabla v^{sn}), \tag{1a}$$

$$\frac{\partial v^{gi}}{\partial t} = \frac{1}{c_m}\left(-I^{gi}_{Na} - I^{gi}_{K} - I^{gi}_{L} - I^{gi}_{T} - I^{gi}_{Ca} - I^{gi}_{ahp} - I_{sn\to gi} - I_{ge\to gi} + I_{giapp}\right) + \nabla\cdot(D_{v^{gi}}\nabla v^{gi}), \tag{1b}$$

$$\frac{\partial v^{ge}}{\partial t} = \frac{1}{c_m}\left(-I^{ge}_{Na} - I^{ge}_{K} - I^{ge}_{L} - I^{ge}_{T} - I^{ge}_{Ca} - I^{ge}_{ahp} - I_{sn\to ge} - I_{ge\to ge} + I_{geapp}\right) + \nabla\cdot(D_{v^{ge}}\nabla v^{ge}), \tag{1c}$$

$$\frac{\partial v^{th}}{\partial t} = \frac{1}{c_m}\left(-I^{th}_{Na} - I^{th}_{K} - I^{th}_{L} - I^{th}_{T} - I_{gi\to th} + I_{smc}\right) + \nabla\cdot(D_{v^{th}}\nabla v^{th}), \tag{1d}$$

where, the symmetric diffusion tensors $D_{v^{sn}}, D_{v^{gi}}, D_{v^{ge}}$ and $D_{v^{th}}$ characterize the spreading of electrical activity from the corresponding nucleus and the last terms in each sub-equations in Eq. (1) represent the diffusion [34]. This diffusion term can capture the random movements of the membrane potentials in the brain used for PD. We use non-negative initial conditions inside the domain Ω and no-flux boundary conditions on the boundary of Ω for v^{sn}, v^{gi}, v^{ge} and vth. The system of Eq. (1) dictates the spread, genesis, and clearance of the membrane potentials of STN, GPi, GPe, and TH neurons throughout the domain Ω in both normal and pathological states. For all of these neurons, $c_m = 1\mu F/cm^2$ is the membrane capacitance. Here, I_L, I_{Na}, I_K are leak, sodium, and potassium spiking currents, respectively. I_T is a low-threshold calcium current, I_{Ca} is a high-threshold calcium current and I_{AHP} is an Ca^{+2}-activated, voltage-independent after hyperpolarization K^+ current. Moreover, h, n, r, c are gating variables associated with I_L, I_{Na}, I_K, I_T and I_{Ca}, and have first-order kinetics governed by differential equations given as follows [12]:

$$\frac{dh^p}{dt} = e_{h^p}[h^p_\infty - h^p]/\tau_{h^p}, \tag{2a}$$

$$\frac{dn^p}{dt} = e_{n^p}[n^p_\infty - n^p]/\tau_{n^p}, \tag{2b}$$

$$\frac{dr^p}{dt} = e_{r^p}[r^p_\infty - r^p]/\tau_{r^p}, \tag{2c}$$

$$\frac{dc^p}{dt} = e_{c^p}[c^p_\infty - c^p]/\tau_{c^p}, \tag{2d}$$

$$\frac{dw^p}{dt} = e_{w^p}(-I_{Ca} - I_T - l_{w^p}w^p), \tag{2e}$$

where $p = sn, gi, ge, th$, and w denotes the intracellular concentration of Ca^{+2} ions and the other relevant parameters are given in Table 1. The reaction kinetics parameters are adopted from an experimental study [53] and the Laplacian of the network is obtained by using HCP data. We have chosen diffusion coefficients as unity for all the membrane potentials to study them mathematically. The Eqs. $(2a)-(2e)$ are required for v^{sn} and Eqs. $(2a), (2b), (2c), (2e)$ are required for v^{gi}, v^{ge}

and Eqs. $(2a), (2c)$ are required for vth. The initial conditions are set to zero for all the gating variables in Eq. (2). The timescale for Eq. (1) and (2) has been chosen to be the same in a bounded domain $\Omega \subset \mathbb{R}^3$. The synaptic current $I_{\alpha\to\beta}$ presented in Eq. (1) represents all synaptic projections from presynaptic cells $\alpha \in \{sn, gi, ge\}$ to postsynaptic cells $\beta \in \{gi, ge, th\}$, and has the following general form:

$$I_{\alpha\to\beta} = g_{\alpha\to\beta}(v^{\alpha} - E_{\alpha\to\beta}) \sum_{k} S_{\alpha}^{k}, \tag{3}$$

where $g_{\alpha\to\beta}$ represents the maximum synaptic conductance, and E represents the reversal potential. The sum in Eq. (3) shows the overall presynaptic cells adopted from [12]. In the next section, we develop a discrete brain network model of cortex–BGTH based on the continuous model presented here. The idea is to highlight the connecting nodes of brain regions involved in the healthy and PD states. Moreover, a specific number of nodes has been chosen where the DBS has been applied to treat the affected areas of the brain.

2.2. Discrete brain network model of cortex-BGTH

In this section, we construct a discrete brain network model following the idea of [34] and using brain data from HCP. The network's nodes are defined in the brain connectome, which is often correlated with well-known areas from the brain atlas. Our intention is to build a network model such that it can capture the voltage change in time at different nodal points. We use the same reaction kinetics defined in Eq. (1) and the dynamics of gating variables defined in Eq. (2) for the discrete brain network model. Before going to the full network model in the brain connectome, we first define the diffusion terms used in Eq. (1) for the discrete brain network.

The brain connectome can be represented as a weighted network $\mathcal{G}$ with V nodes and E edges derived from DTI and tractography [34,54–56] has been adopted from HCP. This network's edges depict axonal bundles in white-matter tracts. A weighted graph Laplacian has been used to generate a network approximation of the diffusion terms in the system of Eqs. (1), which have the generic form $\nabla \cdot (D_v \nabla v)$ or similar. The ratio of mean fiber number n_{ij} to mean length squared, l_{ij}^2, connecting nodes i and j is chosen as the weights of the weighted adjacency matrix $\mathbf{W}$, which is used to generate the graph Laplacian given as follows:

$$W_{ij} = \frac{n_{ij}}{l_{ij}^2}, \quad i, j = 1, \dots, V. \tag{4}$$

The weights used above are compatible with the inverse length-squared dependency seen by canonical discretization of the continuous Laplace (diffusion) operator in the system of Eqs. (1). The diagonal matrix with elements is the weighted degree matrix

$$D_{ii} = \sum_{j=1}^{V} W_{ij}, \quad i = 1, \dots, V. \tag{5}$$

In addition, we define the graph Laplacian $\mathbf{L}$ with (i, j)-entry as

$$L_{ij} = \rho(D_{ij} - W_{ij}), \quad i, j = 1, \dots, V, \tag{6}$$

where ρ is the diffusion coefficient. The simulation's adjacency matrix is constructed from the tractography of diffusion tensor magnetic resonance images belonging to 418 healthy people from the Human Connectome Project [57] as provided by Budapest Reference Connectome $v3.0$ [58,59]. Eqs. (4)–(6) are adopted from [34]. Fig. 1 depicts a network with $V = 4$ nodes and $E = 6$ edges corresponding to the brain regions of the putamen, globus pallidus, and thalamus. We assume that each one of the nodes covers a surface area of 1.5 cm^2. The dynamics of each node associated with STN, GPi, GPe and TH carries the voltage v^{sn}, v^{gi}, v^{ge} and vth, respectively. Let v_1, v_2, v_3 and v_4 be the membrane potentials of STN, GPi, GPe, and TH neurons in the brain regions. The network equations corresponding to the continuous model then take the form of a system of first-order ordinary differential equations as follows:

$$\frac{dv_1}{dt} = -d_{v^{sn}} \sum_{k=1}^{V} L_{1k} v_k + \frac{1}{c_m}\Big(- I_{Na}^{sn} - I_{K}^{sn} - I_{L}^{sn} - I_{T}^{sn} - I_{Ca}^{sn} - I_{ahp}^{sn} - I_{ge\to sn} + I_{snapp}\Big), \tag{7a}$$

$$\frac{dv_2}{dt} = -d_{v^{gi}} \sum_{k=1}^{V} L_{2k} v_k + \frac{1}{c_m}\Big(- I_{Na}^{gi} - I_{K}^{gi} - I_{L}^{gi} - I_{T}^{gi} - I_{Ca}^{gi} - I_{ahp}^{gi} - I_{sn\to gi} - I_{ge\to gi} + I_{giapp}\Big), \tag{7b}$$

$$\frac{dv_3}{dt} = -d_{v^{ge}} \sum_{k=1}^{V} L_{3k} v_k + \frac{1}{c_m}\Big(- I_{Na}^{ge} - I_{K}^{ge} - I_{L}^{ge} - I_{T}^{ge} - I_{Ca}^{ge} - I_{ahp}^{ge} - I_{sn\to ge} - I_{ge\to ge} + I_{geapp}\Big), \tag{7c}$$

$$\frac{dv_4}{dt} = -d_{v^{th}} \sum_{k=1}^{V} L_{4k} v_k + \frac{1}{c_m}\Big(- I_{Na}^{th} - I_{K}^{th} - I_{L}^{th} - I_{T}^{th} - I_{gi\to th} + I_{smc}\Big), \tag{7d}$$

with non-negative initial conditions for all the variables v_1, v_2, v_3 and v_4. Also, $d_{v^{sn}}, d_{v^{gi}}, d_{v^{ge}}$ and $d_{v^{th}}$ are the diffusion terms corresponding to each node. It is noteworthy that without the first term, Eqs. (7) follow Ohm's law [12]. The weights of the weighted adjacency matrix are motivated by the spread of transneuronal degeneration from a node to its neighbors. Each region serves as both a node in functional brain networks and a region of interest (ROI). By studying significant connections and nodes chosen by a discrete brain network model (on a large scale), we may explore the biological characteristics of these relationships between ROIs. Further, we focus on the effect of DBS on the cortex–BG–thalamus loop in small and large-scale brain networks in the next Section 2.3.

2.3. Deep brain stimulation

DBS is the use of persistent electrical stimulation of the brain via an implanted electrode for therapeutic purposes. It is most frequently used to treat the motor symptoms of PD, essential tremor, and dystonia, but it is also being studied to treat a wide range of neurological and psychiatric diseases such as epilepsy, obsessive-compulsive disorder, and severe depression [14]. Moreover, the BGTH neurons and sub-network brain models successfully propose underlying processes for improving PD hypokinesia symptoms following DBS [6,12,38]. However, they are insufficient in defining the plethora of additional effects that DBS may have on PD patients, such as stiffness, tremor, and cognitive or behavioral abnormalities [37,60]. The most widely used DBS device involves stereotactically implanting a four-contact stimulating electrode in the target and connecting it through a subcutaneous cable to a pacemaker-like unit called an implantable pulse generator (IPG) that is positioned on the chest wall behind the collarbone. Although electrodes are normally put bilaterally, clinical circumstances may necessitate unilateral stimulation. Deep brain regions (including deep white matter pathways) are more commonly targeted than cortical locations. A therapist adjusts the stimulation settings using a portable device that wirelessly communicates with the IPG, tailoring stimulation to maximum symptom alleviation while minimizing adverse effects [14]. As a result, the important step in understanding DBS effects should be to expand the local DBS effects of the cortex–BG–thalamus loop to small and large-scale brain networks. Therefore, we have applied the DBS stimulus to the BGTH brain network for both the temporal and the spatio-temporal (i.e., the discrete brain network) models. Numerous symptoms react to DBS with different time courses in the treatment of movement disorders and mental conditions. The ventral intermediate thalamus DBS for essential tremor relieves tremor in seconds [14].

DBS to the STN for PD relieves tremors in seconds, stiffness and bradykinesia in minutes to hours and axial symptoms in hours or days. Likewise, the time it takes for symptoms to return after STN DBS has been turned off is similar to the time it takes for symptoms to disappear after stimulation has been switched on. In dystonia, DBS to the GPi can result in an immediate improvement in phasic dystonic movements, although tonic symptoms take months to develop [1]. The nigrostriatal tract (NST), which connects the STN and striatum, is one of the primary dopaminergic routes and has been demonstrated to be clinically useful in visualizing the architecture of the healthy human brain as well as targeting DBS [61]. Importantly, STN is the most often utilized DBS target for PD [14], and GPi is also considered a therapeutically useful stimulation target [12]. So, GPi and STN are chosen as the target for stimulation on dynamic (temporal) and discrete brain (spatio-temporal) network models in this study. Therefore, Fig. 1 illustrates the typical placement of a DBS electrode in the STN and GPi neurons. The DBS is modeled as [9,19]:

$$I_{DBS} = i_D H(\sin(2\pi t/\rho_D)) \cdot [1 - H(\sin(2\pi(t+\delta_D)/\rho_D))], \tag{8}$$

where $i_D = 200\ \mu A/cm^2$ is the stimulation amplitude, chosen here for numerical simulations, $\delta_D = 0.6$ ms is the length of each impulse and $\rho_D = 6$ ms is the stimulation period [9]. Importantly, as an alternative to DTI, diffusion tensor tractography is a multiscale discrete brain network model that allows for the detection of damaged dopaminergic pathway connections, which may help in the early identification of PD. Hence, the DBS current is added into the model presented in Sections 2.1–2.2 both in temporal and spatio-temporal models to the membrane potential equations of each STN and GPi neuron directly, for example, the STN equation in temporal and spatio-temporal domains is modified as follows:

$$\frac{dv_1}{dt} = \frac{1}{c_m}\left(-I_{Na}^{sn} - I_K^{sn} - I_L^{sn} - I_T^{sn} - I_{Ca}^{sn} - I_{ahp}^{sn} - I_{ge\to sn} + I_{snapp} + I_{DBS}\right), \tag{9}$$

$$\frac{dv_1}{dt} = -d_{v^{sn}} \sum_{k=1}^{V} L_{1k} v_k + \frac{1}{c_m}\left(-I_{Na}^{sn} - I_K^{sn} - I_L^{sn} - I_T^{sn} - I_{Ca}^{sn} - I_{ahp}^{sn} - I_{ge\to sn} + I_{snapp} + I_{DBS}\right), \tag{10}$$

where $c_m = 1\ \mu F/cm^2$ for I_{DBS} [12]. According to Eq. (10), the DBS electrode has been applied to the STN node in the discrete brain network connectome. Moreover, a reliability index (RI) is employed in the computation to assess the relay reliability of TH as in [12]:

$$RI = 1 - \frac{N_{error}}{N_{SMC}}, \tag{11}$$

where N_{error} represents the total number of errors in thalamic transmission. Three categories of errors were considered: misses, bursts, and spurious events. A failure occurred when a neuron did not spike, a burst occurred when a neuron spiked repeatedly with a single stimulating pulse, and a spurious event occurred when the thalamic neuron spiked in the absence of SMC input [12]. Here, the thalamic neuron spike is recognized as transmembrane voltage surpassing a threshold of −35 mV. The total number of SMC input is denoted by N_{SMC}. The greater the value of RI, the better the performance of the relay reliability.

Eventually, the overall multiscale brain network computational modeling is utilized in this work to reveal the effects of DBS during resting-state fMRI in patients with PD. Specifically, we investigate the local and global influence of DBS on the formation of asynchronous, stable, or critical oscillatory states time-continuous discrete brain network model [62]. In summary, we provide a novel continuous model of the BGTH network mediated by diffusion terms, as well as a discrete brain network model of the BGTH system with a focus on Laplacian terms. Furthermore, we used whole-brain computational modeling on the dataset from HCP to track changes in STN-GPi functional connectivity along with DBS. Finally, based on these models, we will discuss the simulation results under healthy and pathological states in Section 2 but before we first discuss the dynamics of action potentials of the BGTH brain network.

2.4. Dynamics of action potentials involved in BGTH brain network

The temporal and spatio-temporal dynamics of the brain involve a large (i.e., billions of neurons supposed to be equal to 100 neurons) set of neurons in both modeling approaches. It is noteworthy that neurons communicate with each other through action potentials, and the junction between two neurons is called a synapse. For example, neuron A releases a chemical neurotransmitter in response to an action potential in neuron B. The neurotransmitter can either aid (excite) or hinder (inhibit) neuron B from firing its action potential. The balance of hundreds of excitatory and inhibitory inputs to a neuron determines whether an action potential is produced in an intact brain. Importantly, in the brain network neurons can be considered electrical devices at their core. The cell membrane (the border between a cell's interior and exterior) has many channels that allow positive and negative ions to flow into and out of the cell. The interior of a cell, for example, the BG regions, is often more negative than the outside; neuroscientists estimate that the inside is around −70 mV less negative than the outside or that the cell's resting membrane potential is −70 mV [12]. Hence, we have considered the resting membrane potential of STN, GPi, GPe, and TH to be approximated by −65 mV for the present study. In addition, the potential of the membranes in the brain is not fixed. It fluctuates regularly, mostly due to inputs from other neurons' axons. Some inputs cause the membrane potential of the neuron to increase (for example, from −70 mV to −65 mV), whereas others cause it to decrease [63]. Depending on whether they stimulate or inhibit the production of action potentials, they are referred to as excitatory or inhibitory inputs. The schematic representation of action potentials involved in the neural mechanism is presented in Fig. 2. Action potentials referred to as "spikes" are the basic units of communication between neurons, and they occur when the sum of all excitatory and inhibitory inputs causes the neuron's membrane potential to hit roughly −50 mV, a number known as the action potential threshold [64,65]. In the threshold state, positive (e.g., Na^+, K^+, Ca^+) or negative ions (e.g., Cl^-) travel through channels that span the membrane. We have considered that each of these ions is associated with respective currents and is involved in the BGTH brain network.

The fact that a neuron creates and controls action potentials contributes significantly to its susceptibility to PD [66,67]. Their anatomical structure and spontaneous tonic activity determine these needs. Each substantia nigra pars compacta dopaminergic (DASNc) neuron produces numerous synapses that target and coordinate the activity of geographically scattered networks in the striatum [66,67]. Each of the 382,000 DASNc neurons in the human brain has an estimated total length of around $4.5m$ and produces between 1 and 2.4 million synapses [66]. When there is a threshold due to increased action potential, these neurons need more energy to come back into the normal state. The loss of dopaminergic neurons in the brain is regarded to be a crucial factor in PD progression. Because of their vast branching and the enormous amounts of energy necessary to convey nerve impulses over this broad network, these neurons are prone to degeneration. Pacemaking neurons are dopaminergic neurons. This implies that they are continually discharging rhythmically, necessitating a significant amount of energy to recharge. When neurons run out of energy, they deteriorate. Studies are currently being conducted to reduce the energy needs of these neurons to protect them and prevent the development of PD [16,64,68]. Based on the ideas highlighted here, we focus on the action potentials and firing patterns of STN, GPi, GPe, and TH neurons of the BGTH model in the temporal and spatio-temporal dynamics in

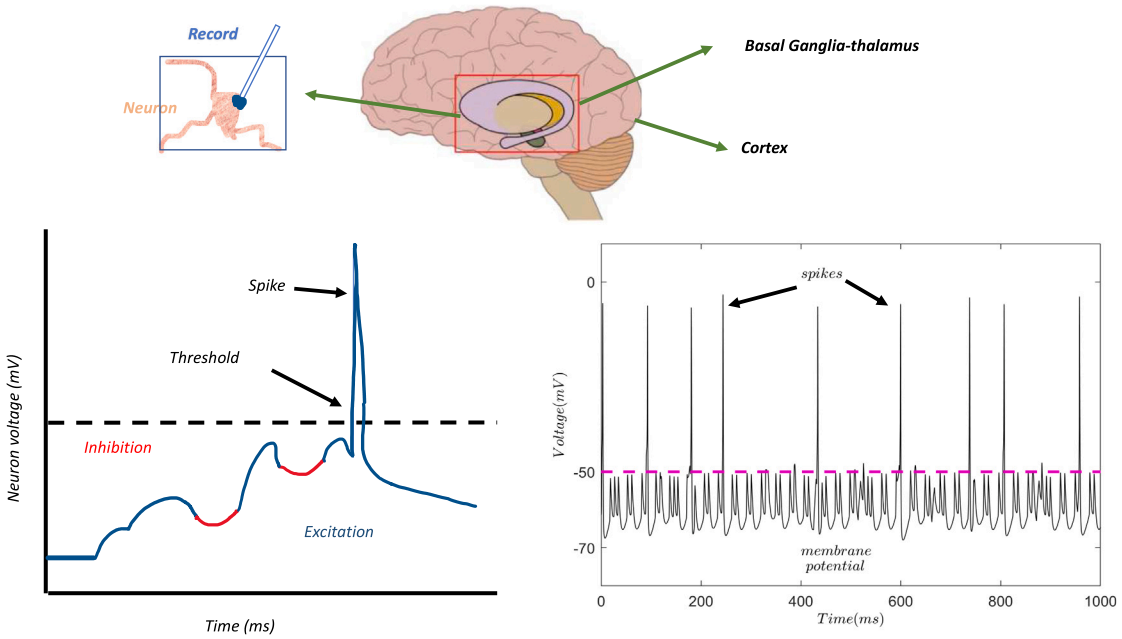

Fig. 2. (Color online) Schematic diagram of a brain network and a neuron spikes when the total of its excitation and inhibition exceeds a certain threshold. The bottom right image has been developed from a neuron in the brain cortex.

the coming Section 3.2–3.2. The STN, GPi, and GPe neurons fire randomly in a healthy state, and the TH can properly transfer sensorimotor cortical signals. The firing patterns of the GPe and GPi cells fluctuate significantly in the Parkinsonian state, and they are characterized by high-frequency bursting oscillations. In contrast, TH neurons are unable to correctly transfer cortical signal input.

3. Results

3.1. Temporal dynamics of cortex-BGTH brain network

In this section, we present the novel results for the temporal model of (1) by neglecting the Laplacian term. In both normal and pathological situations, the BGTH network can define alterations in firing rates that are consistent with experimental observations [12,16].

The firing patterns of STN, GPi, GPe and thalamic neurons in different states of the BGTH network are shown in Figs. 3 and 4. In normal conditions, STN, GPi, and GPe neurons all exhibit tonic spiking activity, and the TH reacts accurately to the excitatory SMC input, resulting in a single action potential in each TH neuron, as illustrated in Fig. 3. The high frequency and erratic inputs from GPi do not compromise the thalamic relay reliability in this scenario. We applied a strong stimulus to maintain the resting membrane potential of the brain as evident from Fig. 3. It can be seen that an external stimulus can push the membrane potential to a specific threshold value in BG and the thalamus, although this can be varied by tissue. At this stage, I_{ahp}, i.e., the Ca^{+2} activated after hyperpolarization K^{+} current maintained the ionic homeostasis in the brain. Finally, when the K^{+} channels are closed, the neurons return to their resting membrane potential. Therefore, the external stimulus (I_{snapp}, I_{giapp}, and I_{geapp} in Eq. (1)) helped ions to maintain the resting membrane potential in the thalamus and BG, in the healthy state as shown in Fig. 3.

However, the Parkinsonian state is simulated by lowering the constant bias currents I_{app} applied to the STN, GPe, and GPi, as shown in the Table 1 (pd is a parameter, and $pd = 0$ indicates that the network is in normal states, while $pd = 1$ shows that the network is in Parkinsonian states). The findings are comparable with what has been reported in patients with PD [12,19,53], as illustrated in Fig. 4 (black color), where bursting behavior and synchronization occur in the STN and GPi neurons. It is evident from Fig. 4 (black color) that the external stimulus in the PD state decreases the oscillations of the membrane potential of STN and GPi neurons and increases the number of spikes in the BG and thalamus brain network, as compared to a healthy state (see Fig. 3). An increased number of spikes damage the normal functioning of neurons, and the brain goes into a disease state. There is also a threshold in the action potentials of STN and GPi neurons. In addition, the sum of all the excitatory and inhibitory inputs makes the neuron's membrane potential reach around −50 mV (see black color in Fig. 4). We compute the RI in both normal and Parkinsonian conditions. The value of RI in the normal condition is 0.9974. However, with PD, the value of RI lowers to 0.5113, a drop of over 50 percent. In this situation, STN and GPi's synchronous and bursting output is strong enough to alter thalamic activity. The TH neurons can no longer reliably relay the SMC input, and the relay reliability is harmed by excessive bursts and missing pulses in the Parkinsonian state. Although thalamic relay reliability is associated with the efficacy of symptom alleviation in animal models of PD and the degree of bradykinesia in people with PD [69,70], it is regarded as a reliable predictor of treatment efficacy.

Previous research has shown that open-loop DBS-STN stimulation can increase the relay reliability of TH neurons [9,12]. However, the GPi is also recognized as a therapeutically useful target for stimulation [3]. Because the inhibitory waveform from the GPi to the TH has a significant impact on relay reliability, directly modulating the GPi inhibitory waveform via GPi stimulation makes the effect of stimulation on relay reliability more predictable. However, we have considered both STN and GPi as the target for stimulation in this study. Importantly, as depicted in Fig. 4, the DBS is applied to STN and GPi neurons during $t = 500$ ms $- 1500$ ms presetting in red color. Fig. 4 (top) shows the results after a typical placement of a DBS electrode in the sub thalamus, i.e., the STN node, the most often treated DBS target for PD [14]. It is reported that open-loop DBS-GPi (Fig. 4-bottom) totally restores the relay reliability of TH neurons to SMC input [12]. Additionally, the DBS stimulus would replace bursting patterns of GPi and STN neurons by tonic spiking as shown in Fig. 4.

Moreover, we found that when the DBS is applied to STN neurons, the value of RI is equal to 0.9410, and when the DBS is applied to GPi

Table 1
Parameter set for the BGTH network (modified from [53]).

	STN neuron	GPe/GPi neuron	TH neuron
e_h	0.75	0.05	1
e_n	0.75	0.1	0
e_r	0.2	1	1
e_c	0.08	0	0
e_w	3.75×10^{-4}	1×10^{-4}	0
I_L	$2.25(v+60)$	$0.1(v+65)$	$0.05(v+70)$
I_K	$45(n^4)(v+80)$	$30(n^4)(v+80)$	$5((0.75(1-h))^4)(v+75)$
I_{Na}	$37(m_\infty(v))^3 h(v-55)$	$120(m_\infty(v))^3 h(v-55)$	$3(m_\infty(v))^3 h(v-50)$
I_T	$0.5(a_\infty(v))^3(b_\infty(r))^2(v-140)$	$0.5(a_\infty(v))^3 r(v-120)$	$5(p_\infty(v))^2 rv$
I_{Ca}	$2(c^2)(v-140)$	$0.15(s_\infty(v))^2(v-120)$	–
I_{ahp}	$20(v+80)(w/(w+15))$	$10(v+80)(w/(w+10))$	–
$I_{ge\to sn}$	$0.5S_{ge\to sn}(v+85)$	–	–
$I_{ge\to ge}$	–	$0.5Sge \to ge(v+85)$	–
$I_{ge\to gi}$	–	$0.5S_{ge\to gi}(v+85)$	–
$I_{sn\to ge}$	–	$0.15S_{sn\to ge}v$	–
$I_{sn\to gi}$	–	$0.15S_{sn\to gi}v$	–
$I_{gi\to th}$	–	–	$0.112S_{gi\to th}(v+85)$
$n_\infty(v)$	$1/(1+exp(-(v+32)/8.0))$	$1/(1+exp(-(v+50)/14))$	–
$m_\infty(v)$	$1/(1+exp(-(v+30)/15))$	$1/(1+exp(-(v+37)/10))$	$1/(1+exp(-(v+37)/7))$
$h_\infty(v)$	$1/(1+exp((v+39)/3.1))$	$1/(1+exp((v+58)/12))$	$1/(1+exp((v+41)/4))$
$a_\infty(v)$	$1/(1+exp(-(v+63)/7.8))$	$1/(1+exp(-(v+57)/2))$	–
$b_\infty(r)$	$1/(1+exp(-(r-0.4)/0.1)) - 1/(1+exp(4))$	–	–
$r_\infty(v)$	$1/(1+exp((v+67)/2))$	$1/(1+exp((v+70)/2))$	$1/(1+exp((v+84)/4))$
$s_\infty(v)$	–	$1/(1+exp(-(vs+35)/2))$	–
$c_\infty(v)$	$1/(1+exp(-(v+20)/8))$	–	–
$p_\infty(v)$	–	–	$1/(1+exp(-(v+60)/6.2))$
$\tau_h(v)$	$1+500/(1+exp((v+57)/3))$	$0.05+0.27/(1+exp(-(v+40)/-12))$	$1/(\alpha_h(v)+\beta_h(v))$
$\alpha_h(v)$	–		$0.128exp(-(v+46)/18)$
$\beta_h(v)$	–		$4/(1+exp(-(v+23)/5))$
$\tau_n(v)$	$1+100/(1+exp((v+80)/26))$	$0.05+0.27/(1+exp(-(v+40)/-12))$	–
$\tau_r(v)$	$7.1+17.5/(1+exp((v-68)/2.2))$		$0.15(28+exp(-(v+25)/10.5))$
$\tau_c(v)$	$1+10/(1+exp((v+80)/26))$	–	–
I_{snapp}	$33-10pd$	–	–
I_{giapp}		$22-6pd$	–
I_{geapp}		$21-13pd+(-1.5)$	–

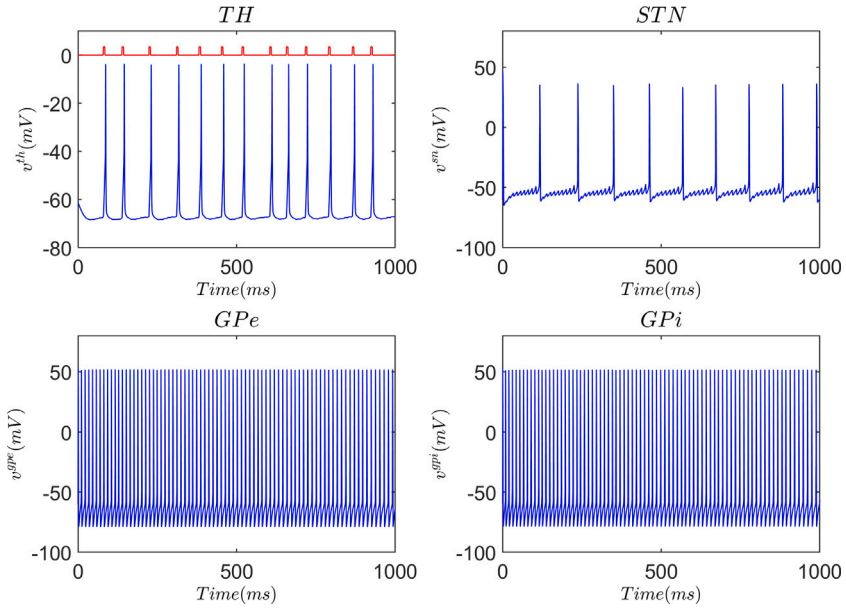

Fig. 3. Membrane voltages of the TH (top right), STN (top left), GPe (bottom right) and GPi (bottom left) neurons in a healthy state. The red pulse trains in the top right panel denote SMC signals. (For interpretation of the references to color in this figure legend, the reader is referred to the web version of this article.)

neurons, the value of RI is equal to 0.9102. Therefore, there is no doubt to say that DBS-STN is proven to be an effective treatment for PD, and DBS-STN stimulation can improve TH relay reliability validated by the recent experimental studies [13,71]. Now the important thing here is to discuss what happens when the DBS is turned off. We have highlighted this part in blue color as shown in Fig. 4. This is the healthy state of the neurons that showed up after the DBS is applied for the treatment of PD. Interestingly, it is shown that the number of spikes is reduced, and there are more oscillations in the membrane potentials of STN and GPi neurons in the BGTH brain network after the DBS is applied. Hence, the number of spikes is less in blue color as compared to black color as depicted in Fig. 4. The time period defined for the overall PD and healthy state is 0 ms – 4000 ms. Moreover, excitation and inhibition of neurons are frequent, and the results are consistent as shown in Fig. 3,

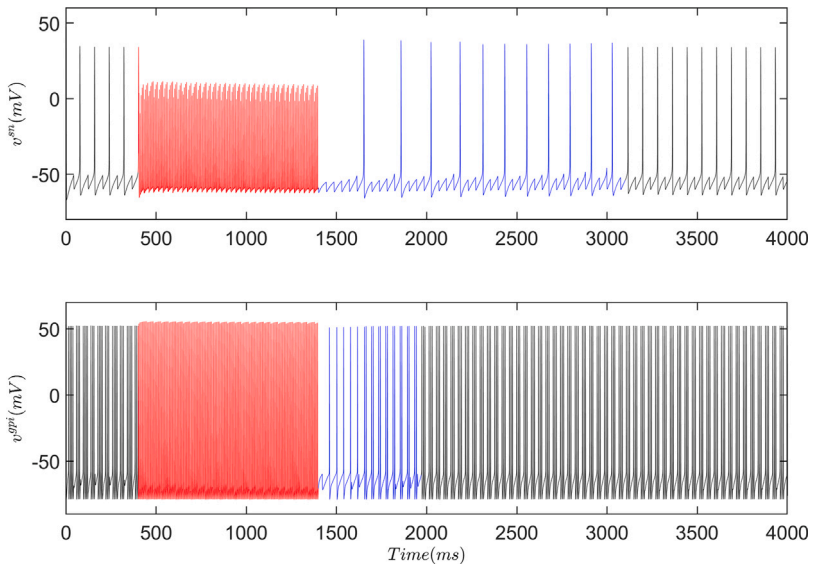

Fig. 4. Membrane voltages of the STN (top) and the GPi neurons in the Parkinson's state (black color). The effects of open-loop DBS on the STN and GPi neurons are presented in red color. However, the blue color shows the healthy state after the DBS is applied to the PD state. (For interpretation of the references to color in this figure legend, the reader is referred to the web version of this article.)

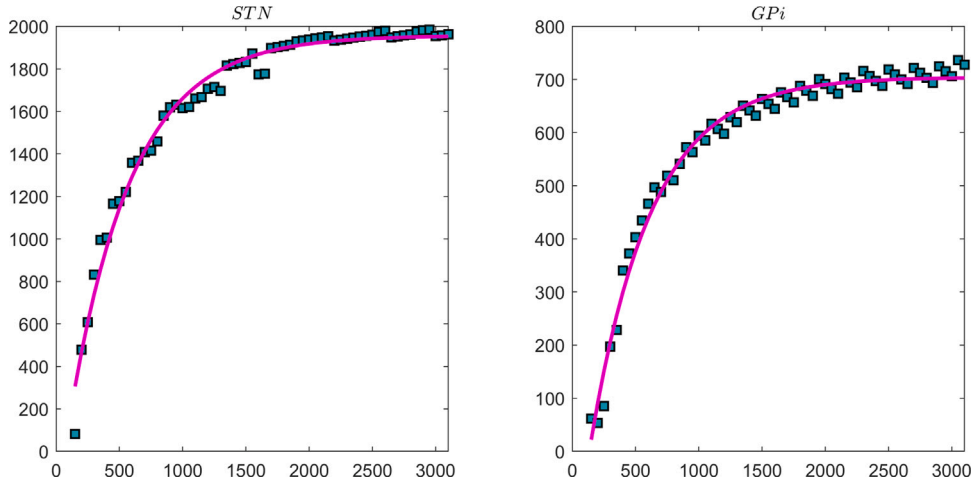

Fig. 5. The predictability of time to repeat the dynamics before the DBS with respect to the DBS-time applied to STN (left) and the GPi (right) neurons (x-axis corresponds to the time interval presented in red color in Fig. 4, and the y-axis corresponds to the time interval presented in blue color in Fig. 4 for both STN and GPi neurons). (For interpretation of the references to color in this figure legend, the reader is referred to the web version of this article.)

for healthy state [19]. We can clearly see that STN neurons maintained the healthy state more often (i.e, up to 3100 ms) than GPi neurons (i.e., up to 1900 ms) after the DBS is applied, as depicted in Fig. 4.

We have fitted the curve (using the least-square method) for the healthy state that appeared after DBS stimulation has been applied as presented in Fig. 5. We predicted that if we apply the DBS in the range of 500 ms – 1500 ms and then turn it off, the brain maintained a healthy state until 0.05 ms for STN neurons and 0.035 ms for GPi neurons (dynamics of ten neurons in each nucleus resulted in the same trends described for the results with fifty or more neurons). To the best of our knowledge, these are the novel results so far for the temporal dynamics of the Cortex–BGTH brain network. Our prediction is accurate in the sense that STN appears to be more effective than GPi neurons [6,19,53]. The predictability of a healthy state after the DBS off-rate in regard to Fig. 5, we found that R^2-value appears to be 0.98371 for STN neurons and 0.98567 for GPi neurons displayed with 95% confidence intervals. These findings suggest the STN's involvement in several interconnected activities, including transitioning from automatic to regulated processing, inhibitory and executive control, altering response thresholds, and impacting speed–accuracy trade-offs validated with studies [72,73]. Such STN DBS-induced inhibitory and executive control deficiencies may contribute to some of the psychological difficulties observed by a proportion of operated cases following STN-DBS surgery in PD.

3.2. Dynamics of cortex-BGTH brain network in spatio-temporal domain

In the present section, we present the results in the spatio-temporal domain based on the model developed in Section 2.1–2.2. To connect the discrete brain network nodes and the spiking network simulator, we needed to assign diffusion parameters for the paths between the BGTH regions and the cortex. To personalize the normative connectome, we have added the network among the BG and thalamus regions with the continuous Laplacian operator for the healthy and PD states, respectively. This 'hybrid' connectome constituted normative diffusion parameters among the cortex regions and between cortex and BGTH but included individually fitted membrane voltages for the spiking network of the BGTH. For the presentation and for determining the couplings between the two scales (i.e., temporal and spatio-temporal dynamics

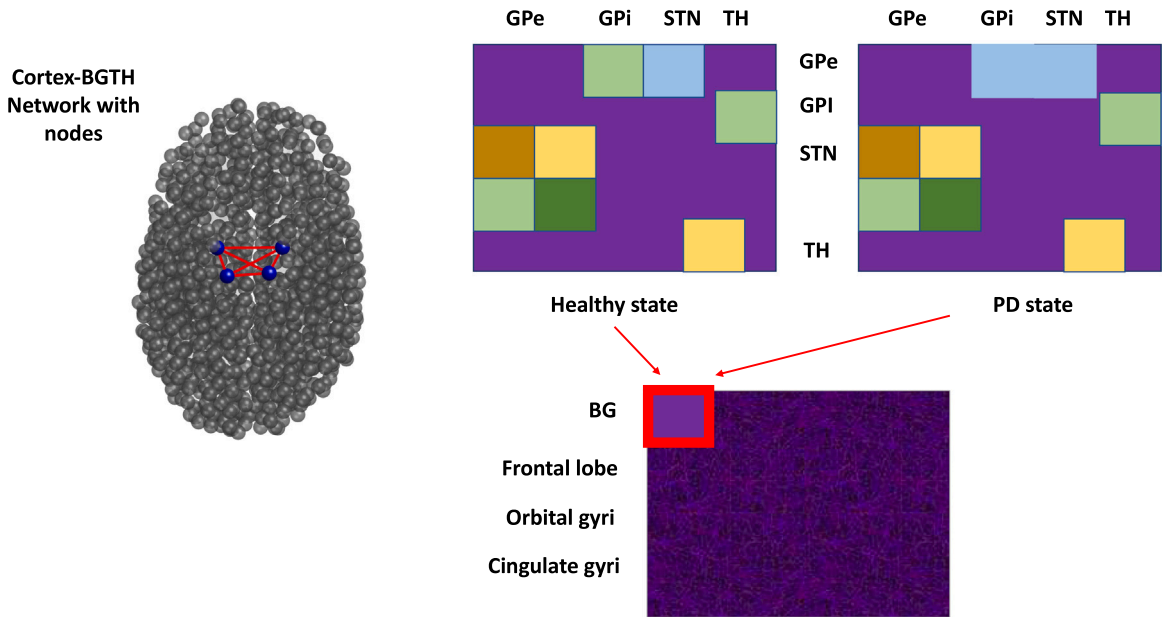

Fig. 6. Discrete brain network connectome in the healthy state (left) (axial view from below). The optimally fitted brain graph data from HCP within BG connection inside the connectome (red square). Each entry in any of the three colored matrices represents the normalized number of streamlines that start in the region marked on the vertical axis and end in the region marked on the horizontal axis. The four nodes are STN, GPe, GPi, and TH, and we replaced the spiking node "cortex" with the whole brain connectomic model. (For interpretation of the references to color in this figure legend, the reader is referred to the web version of this article.)

described in Sections 2.1 and 2.2), we adjusted the nodes for the STN, GPe, GPi and TH corresponding to the putamen, globus pallidus and thalamus, brain regions as shown in Fig. 6. We used tract data from HCP to include a fine-grained parcellation for the BGTH and cortex atlas and detailed data of their pathways to and from the cortical regions because of its current use for clinical DBS planning. While [18] used the motoric parts of the BG regions only, we used the complete BG regions as a first approach. The SMC signal was applied to the cortex. In the multiscale modeling approach, we replaced the spiking node "cortex" with the whole brain connectomic model (cortex–BGTH model presented in Eqs. (7)), as shown in gray color in Fig. 6. Whereas, the blue color represents the STN, GPi, GPe and TH nodes in the whole brain and these nodes are connected through diffusion (red color). This procedure resulted in a whole-brain matrix for the pathways between the cortex and the BGTH regions.

Fig. 7 shows the healthy state of the brain in the presence of diffusion based on the discrete brain network model presented in Section 2.2. As depicted in Fig. 7, electrical stimulation of the motor cortex, e.g., SMC signal causes triphasic changes in GPi activity. On average, a fast excitation of GPi is observed approximately 8 ms after stimulation of the primary motor cortex, followed by a short inhibition at approximately 21 ms after stimulation and a late excitation at approximately 30 ms after stimulation validated from [5,74]. It is important to note that the hyper direct pathway causes fast excitation, the direct pathway causes short inhibition, and the long indirect pathway causes late excitation in parallel recordings in STN and GPe neurons [5]. The hyper direct pathway's exceptionally fast response has been linked to the special characteristics of STN neurons, which include a slow decay of excitatory postsynaptic potentials (EPSPs) and a dynamic decrease in spike threshold after EPSPs. We found that, in regards to Fig. 7, there are many oscillations in the TH and STN neurons in the presence of diffusion as compared to Fig. 3. Moreover, we observed more excitation and fewer spikes in the STN and TH when the SMC signal is applied. It is validated from the experimental study such as in monkeys, striatal neurons arborize with a high degree of specificity in the globus pallidus, whereas STN neurons more evenly excite vast numbers of pallidal cells [66]. Despite their differing arborization patterns, striatal and subthalamic cells in the internal and external regions of the globus pallidus converge upon the same pallidal neurons. Based on this evidence [66], the direct and short indirect pathways are thought to impact pallidal representations that are relatively focused, but the hyper direct and long indirect pathways are thought to have more broad effects [7,75]. Therefore, the electrical activity of TH neurons in the presence of diffusion is enhanced when the external stimulus is applied even in a healthy state. Hence DTI allows for the detection of damaged connections in the dopaminergic pathway and may aid in the early diagnosis of PD. The pathway, which connects the STN and striatum, is one of the major dopaminergic routes and is clinically useful in visualizing the anatomy of the healthy human brain [76], as well as in targeting DBS [61,77].

The membrane voltages of STN, GPi, GPe and TH neurons in a discrete brain network for the Parkinsonian state have been presented in color nodes as shown in Fig. 8. Importantly, the four-color nodes in all pictures are STN (bottom-right), GPi (top-left), GPe (top-right), and TH (bottom-left) neurons in the palladium and thalamus and initially (at $t = 0$) they have the same voltage. We recorded the voltages of all neurons at $t = 354.56$ ms, 356.8 ms, 356.23 ms, 370 ms, 374.67 ms, 383.2 ms, 385.05 ms, 385.57 ms as depicted in Fig. 8. One may get these types of voltages at different times because we have set the time according to our initial conditions and data. Initially, the voltage is −65 mV for all neurons, but there is some randomness in the initial conditions corresponding to voltages and due to diffusion the concentrations of voltages change over time. The color scale of concentrations of voltages in Fig. 8 is plotted using MATLAB jet colormap. For example, at $t = 354.56$ ms, the voltage of GPi neurons is higher than other neurons, and at $t = 356.8$ ms, the voltage of GPe neurons is higher than other neurons in BGTH in the PD state. A similar trend goes for STN, and TH neurons with the time seen in Fig. 8. Finally, the neurons reached the threshold level in the presence of diffusion and synchronization occurs in the PD state. In Fig. 8, the discrete brain network pictures show the concentrations of voltages at $t = 354.56$ ms – 385.57 ms and these trends of voltages repeat themselves after every cycle. The higher concentrations of voltages disrupt the electrical activity of the brain, and the PD state occurs. Traditionally, this behavior and dynamics of electrical voltages and alterations in neural firing rates underlie the BG dysfunctions leading to movement disorders [78].

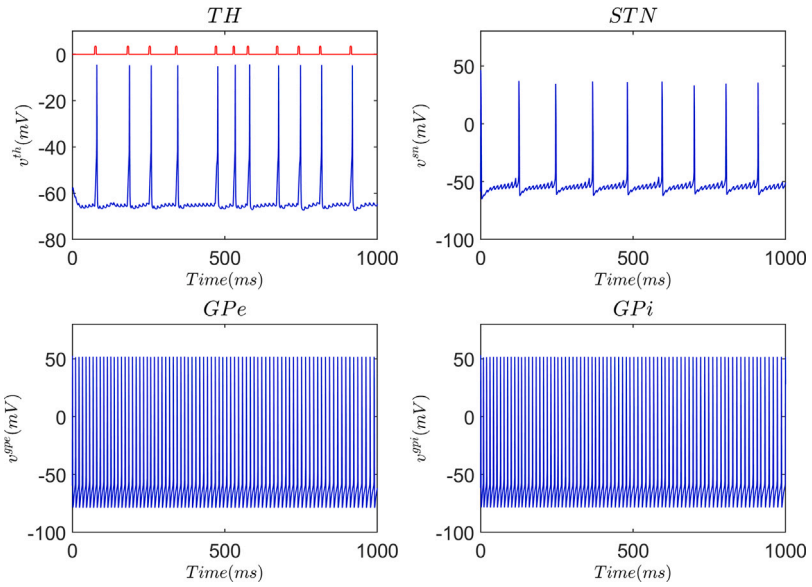

Fig. 7. Membrane voltages of the TH (top right), STN (top left), GPe (bottom right) and GPi (bottom left) neurons of discrete brain network in a healthy state. The red pulse trains in the top right panel denote SMC signals. (For interpretation of the references to color in this figure legend, the reader is referred to the web version of this article.)

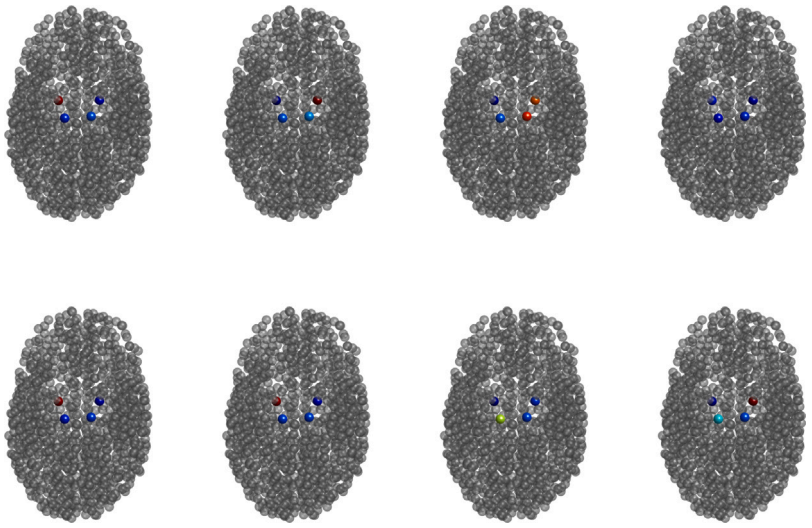

Fig. 8. (Color online) Membrane voltages distributions of STN, TH, GPi and GPe neurons in the brain over time in Parkinson's state (axial views from below). Top panel (left to right): $t = 354.56$ ms, 356.8 ms, 356.23 ms, 370 ms, and for the bottom panel (left to right): $t = 374.67$ ms, 383.2 ms, 385.05 ms, 385.57 ms.

In the case of a multiscale discrete brain network, the DBS stimulus has been applied to STN neurons as presented in Fig. 9 in the PD state. There are large-amplitude jumps in the oscillations of the membrane potential of TH neurons along with a greater number of excitation has been recorded. The number of spikes also reduced in the TH when the DBS has been applied to STN in the PD state. As depicted in Fig. 9, we applied the DBS in a spatio-temporal domain for a smaller amount of time as compared to Fig. 4. It is interesting to know that in the presence of a diffusion operator, neurons maintained a healthy state for a sufficient time after the DBS has been applied. We see the healthy state of STN neurons in blue color as shown in Fig. 9. It is worth noting that the relay reliability of TH neurons to SMC input is restored by open-loop DBS-STN, the bursting patterns of STN neurons are replaced by tonic spiking, and the rhythmic oscillations of the synaptic variable are effectively blocked by DBS.

Similarly, the effect of DBS stimulus on GPi neurons has been presented in Fig. 10. It is noted that in the presence of diffusion, the membrane potential of GPi neurons is higher than in the case of the STN neurons in the PD state. Moreover, we found that when the DBS is applied to the STN node, the value of RI is equal to 0.989, and when the DBS is applied to the GPi node, the value of RI is equal to 0.912. Our findings are consistent with the findings of previous studies [12,79,80]; both found that the RI values of GPi and STN nodes are enhanced in the healthy state with DTI. Again, we found similar trends for discrete brain networks when the DBS is applied to STN and GPi neurons, as shown in Fig. 5. The pattern and behavior of spikes of different colors for STN and GPi neurons (Figs. 9 and 10) are similar as predicted in Fig. 4. Our results support the hypothesis that DBS stops neurons from firing at the stimulation location.

As presented in Fig. 11, we can see how the dynamics of the membrane voltages changed in the presence of diffusion of STN neurons. Importantly, as can be seen from Fig. 11, if we apply the DBS in the time range of 400 ms – 1000 ms and then turn the DBS off. We predicted that the brain maintains a healthy state for a sufficient time. Clearly, increasing the time interval for DBS stimulus will enhance the time duration of a healthy state. Note that we choose 200 ms as a starting time for the DBS stimulus. For instance, Fig. 11 demonstrates the behavior of STN neurons in the presence of diffusion for the novel

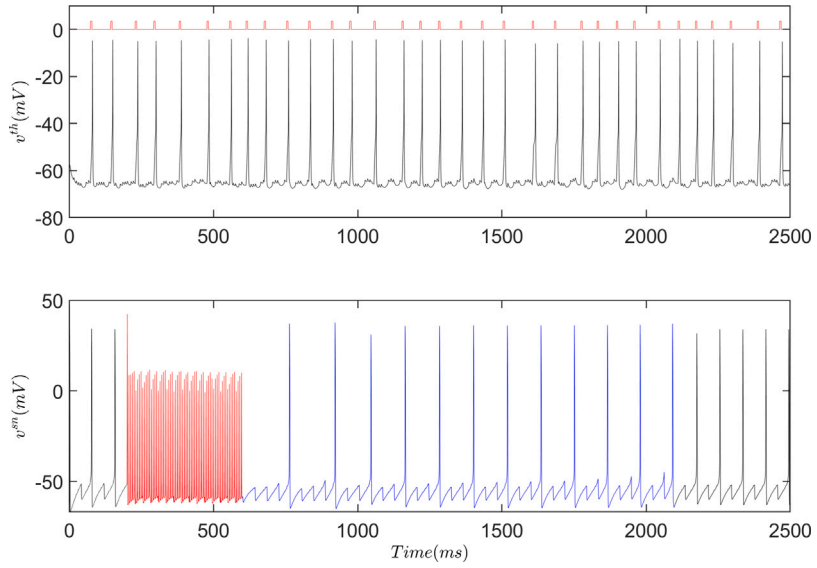

Fig. 9. Membrane voltages of the TH (top) and the STN (bottom) neurons of discrete brain network in the Parkinson's state (black color). The effects of open-loop DBS on the STN neurons are presented in red color (bottom). However, the blue color shows the healthy state after the DBS is applied to the PD state. The red pulse trains in the top panel denote SMC signals. (For interpretation of the references to color in this figure legend, the reader is referred to the web version of this article.)

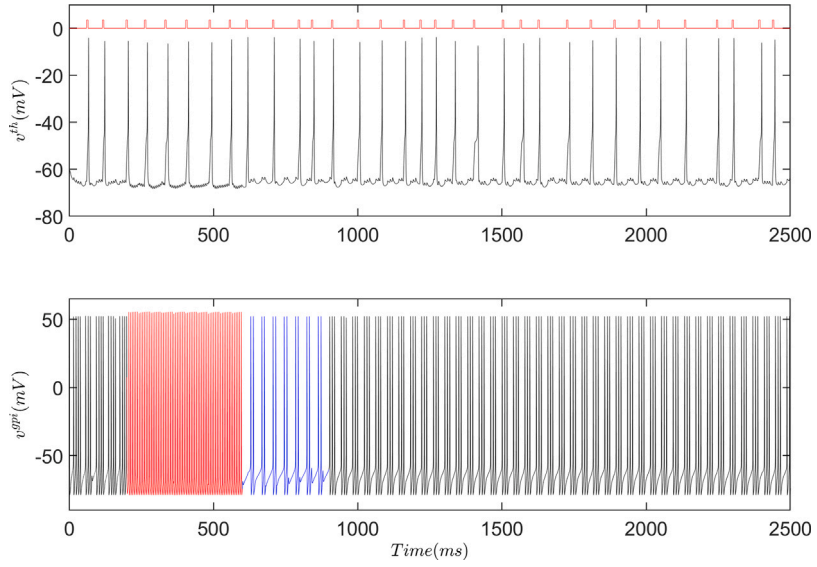

Fig. 10. Membrane voltages of the TH (top) and the GPi (bottom) neurons of discrete brain network in the Parkinson's state (black color). The effects of open-loop DBS on the GPi neurons are presented in red color (bottom). However, the blue color shows the healthy state after the DBS is applied to the PD state. The red pulse trains in the top panel denote SMC signals. (For interpretation of the references to color in this figure legend, the reader is referred to the web version of this article.)

Cortex–BGTH brain network model in the spatio-temporal domain since STN appears to be more effective in the treatment of the PD [6]. We discovered substantial connections between the subthalamic nucleus and the cerebellar cortex, as well as a novel pathway through diffusion operator connecting the dentate nucleus to the internal globus pallidus and the substantia nigra. Regardless of the diffusion transport pathways following our results, time must be allowed for the tracer to reach its target regions in BGTH before proceeding with tracer detection. In this work, we evaluated a new probabilistic tractography-based approach to segmenting GPi and STN nodes in regard to DBS stimulation. We discovered novel results that STN appeared to be more effective for PD patients as compared to GPi in a discrete brain network.

In summary, according to the probabilistic tractography-based approach, accurately estimating many physical and biological systems requires simulating interactions between macroscopic and microscopic phenomena. As a result, massive and large data sets are generated on a variety of temporal and physical scales [81]. To understand how events at one scale affect those at another, it is crucial to visualize data from multiscale simulations using a single integrated tool. We investigate how large-scale simulation patterns affect neural behavior in the context of PD. The main motivation for our study is that diffusion plays a crucial role in the functioning of deep brain structures. PD patients face a poor prognosis despite great advances in imaging, surgery, and radiation therapy. Strong drugs fail when used to treat PD patients because biochemical and physiological barriers reduce drug delivery to the brain. Direct DBS stimulation via specific polymeric devices into the brain has shown good results in both animal models and clinical trials [16,17,31,50,71]. This technique is well-suited and has the potential to provide a sustained level and specifically reach cellular targets in the brain. To establish numerical techniques to validate experimental trends, non-homogeneous diffusion processes in the brain have been extensively studied [34,55,56]. The main goal of this study was to

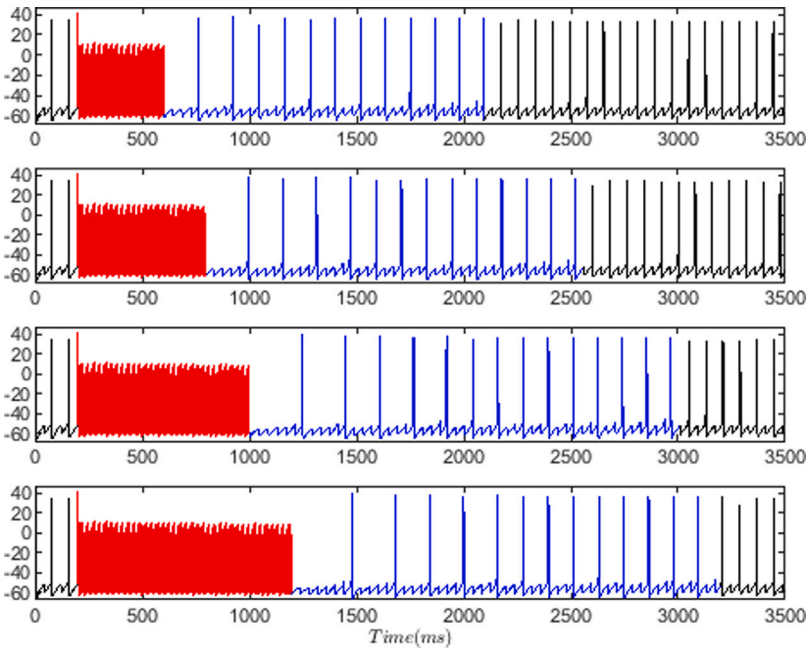

Fig. 11. Membrane voltages of the STN neurons of discrete brain network in the Parkinson's state (black color). The effects of open-loop DBS on the GPi neurons are presented in red color (bottom). However, the blue color shows the healthy state after the DBS is applied to the PD state. The time range of the DBS stimulus is as follows (figures from top to bottom): 400 ms, 600 ms, 800 ms, 1000 ms. (For interpretation of the references to color in this figure legend, the reader is referred to the web version of this article.)

generate an isotropic but inhomogeneous diffusion tensor using MRI and a variety of interpolating functions, each of which was associated with a distinct physical feature at each grayscale level for healthy and pathological states. We discovered parallel trends for both models in the temporal and spatio-temporal domains, demonstrating that adding diffusion to the brain network using mathematical techniques validates experimental trends. To solve the network model numerically, we used Euler's method. We choose $dt = 0.001$ as the time-step, and the results remain unchanged for different time-step values less than the one used. Furthermore, for all simulations, we used fixed brain connectome data (available at https://braingraph.org), and no significant change in time series was seen for other data.

4. Discussion

In general, neurons are the cells that make up our nervous system, and in BG, they are made up of three main nuclei, STN, GPi, and GPe. Neurons use neurotransmitters as a signal to communicate with each other, but they use the action potential to propagate that signal within the cell when the external signal (I_{app}) is applied. Importantly, according to [53], using a lesser number of neurons (e.g., 10 neurons) in each nucleus resulted in the similar patterns mentioned for the results with 100 neurons, so each nucleus of the BG network in the present study consists of 10 cells. Moreover, acquiring accurate data for tracts in the cortex–BGTH brain network is difficult due to structural MRI data's many limitations [37]. Petersen et al. [82] recently published a cutting-edge axonal pathway atlas for the human brain, which combines previous results from histological and imaging data literature with expert knowledge of brain-imaging scientists who collaborated on defining those tracts using a holographic visualization technique. The previous work of [18] optimized the connection probabilities and weights among BG regions per individual to best fit the empirical fMRI data. Because of the difficulties in obtaining and interpreting patient-specific diffusion-weighted imaging data, several research studies have used normative atlases of the human connectome. Yet, it is still unknown if patient-specific connection data might improve the accuracy of such assessments [83]. The existence of weights in BG regions has been established in rat and monkey tracer investigations, as well as human DTI research, notably in connection to the prefrontal cortex, primary motor, and primary sensory cortices [52,84].

In the present study, the temporal model associated with the considered spatio-temporal model in our manuscript is proposed by Lu et al. [12]. In [19], authors modified the traditional Rubin–Terman model to better fit experimental data on neuron firing characteristics. However, the spatio-temporal dynamics of the model are still unexplored experimentally and mathematically, as per our knowledge. The present research focuses on a network mathematical model, which helps experimentalists with some early observations of the membrane potentials of four primary nuclei in the cortex and the BGTH regions [51,52]. Importantly, this paper is based on the visualization of a heterogeneous and substantial data set generated by multiscale, multiphysics simulations in brain regions. To simulate realistic multiscale physical and biological systems, it is increasingly necessary to interface large-scale brain networks with continuum-based models [85]. The direct exterior environment of brain cells is referred to as the ECS. Due to its accessibility to the cell membrane, the structure and composition of the ECS are critical for cellular homeostasis and efficiency. The ECS includes a fluid similar to that found in the ventricles of the brain that maintains an ionic equilibrium for Na^+, Cl^-, Ca^{+2}, and K^+ ions across the cell membrane [86,87]. An ionic balance of this type establishes the cellular resting potential (−65 mV) and allows neuronal action potentials and synaptic transmission to occur. The ECS also acts as a communication channel between cells, allowing chemical impulses to move between them; this is known as volume transmission [88]. In clinical practice, the ECS is a major pathway for drug transport after it has reached the brain [89]. Diffusion is the major mode of substance transport in the ECS, determining both the local and global distribution of numerous ions in the brain [41].

Next, we discuss some of the implications of our findings. Our basic hypothesis is that rhythmic rebound bursts associated with the low-threshold calcium T-current occur in TC cells and probably in cortical motor regions in PD, at least at times when the basal ganglia fires regularly [16]. DBS is expected to lessen these bursts significantly. Furthermore, we anticipate that, in comparison to PD or normal states, firing in at least one of GPi and GPe speeds up and regularizes in DBS, as well as an increase in GPi-GPe associated firing (and with

STN, if STN cells are still firing). We also note that the intensity of feedback inhibition was regulated by an externally applied stimulus for all inhibitory neuronal voltages. Other parameters, such as the intensities of the SMC signal injected into the cortex, remained the same. When a control parameter (e.g., synaptic connections) is pushed over a critical point that defines the boundary of a diffusion process, it triggers a drastic shift in one or more parameters (e.g., firing rates). The average population firing rates were the sole criterion for this second type of tuning, known as feedback inhibition control (FIC), with no regard for prediction quality, which was exclusively reliant on the *pd* parameters set for healthy and Parkinsonian states. With the consideration of prediction quality, FIC modifies the strengths of inhibitory connections, which are needed to compensate for excess or lack of excitement caused by the wide variation in white-matter coupling synaptic strengths that is relevant for the results presented in Fig. 5.

Several processes may be involved in the development of somatic inhibition in white matter [38]. Importantly, surgical recordings from brain data of human participants' GPi [90] and STN [91,92] revealed decreased neuronal spike rates under stimulation (Figs. 9 and 10). In vitro, high-frequency stimulation can cause sustained depolarization of neural membranes, preventing the initiation or propagation of action potentials by inactivating Na^+ channels and increasing K^+ currents (i.e., depolarization block). DBS may also work through a synaptic mechanism, causing inhibitory presynaptic terminals on afferent to the cell body [14]. During GPi stimulation, the time pattern of neuronal inactivation (100 ms after stimulation beginning) supports the idea that inhibition occurs through the release of inhibitory neurotransmitters from striatal and GPe afferents to the GPi [90]. This might also explain why DBS has been observed to elicit local activation rather than inhibition in areas with mainly excitatory input, such as Vim [16] and certain STN neurons [6].

We propose that to understand the mechanism of DBS, we look directly at its influence on populations of neurons and how the population activity is conveyed to populations downstream from the stimulation. Therefore, parts of the BG are either under-stimulated or over-stimulated in PD. DBS in the GPi and the STN, for example, induces alterations in the firing of GPi neurons, but it also causes changes in the thalamic region and, eventually, motor cortex neurons. DBS in the TH will alter motor cortical neurons. Because there are many connections between the TH and the BG, as well as reciprocal connections between the neurons and the TH, the stimulation may have complicated re-entrant consequences. There is no doubt that diffusion is always there to exchange ions between neurons on a microscopic scale. Executive dysfunctions are linked to DTI variables seen in the parietal and frontal areas of the brain [93,94]. PD diffusion characteristics in the parietal and frontal areas are linked to decreased verbal and semantic fluency and visuospatial memory [95]. The diffusion parameter is constant throughout the present study. The GPi and STN are the principal output structures of the BG and have been shown to exhibit an increase in neuronal activity before the beginning of PD motor symptoms in the brain network. GPi-STN-DBS has been used successfully to treat dyskinesias in PD patients with treatment-resistant hyperkinetic movements, tremors, and dystonia [84,96]. Our results are consistent with the experimental studies [80,97]. Even though these approaches have lesser spatial resolution than chemical and viral tract tracing and cannot determine the direction of neuronal pathways, they are the only non-invasive way to investigate anatomical connections in the human brain in real time.

5. Conclusions

We proposed a novel cortex–BGTH model in the spatio-temporal domain for developing a discrete brain network model. This model quantifies the effect of DBS, which is a neurosurgical treatment that treats movement problems associated with PD, essential tremor, dystonia, and other neurological disorders with implanted electrodes and electrical stimulation. In addition, we discussed the co-simulation approach of a cortex–BGTH model for subcortical regions in and around the basal ganglia in the temporal domain. Following that, we obtained data from the HCP for the spatial connections and examined the firing rates of associated neurons on each node in the brain network in a co-simulation environment in the spatial domain. The cortex–BGTH network in both spatial and temporal domains can identify changes in firing rates compatible with experimental results in both normal and pathological situations. The obtained results based on the discrete models suggest that when the DBS is applied to STN and GPi neurons, DBS-STN appears to be more effective than DBS-GPi in the pathological state. In the co-simulation approach, both the original and modified Hodgkin–Huxley models agree qualitatively, and the findings given in this work provide more full knowledge of a unique channel for changing neuronal activity. Moreover, it is worth mentioning that open-loop DBS implanted in the STN neurons restores TH neurons' relay reliability to SMC input. The interesting finding of our study is that DBS in the presence of diffusion would keep STN and GPi neurons in a healthy condition for a sufficient period after the DBS had been given.

For instance, we discovered 34 spikes in the case of GPi neurons in the Parkinson's state when we fixed the time from $0-2000$ ms, without diffusion and without DBS. Also, 22 spikes are used to maintain the healthy state up till the onset of the disease after applying the DBS for a duration of 500 ms to 1500 ms. We observed that, for example, if we set the time from $0-2000$ ms, with diffusion and without DBS, we would get 19 spikes with varying frequencies, and that would take 200 ms before the DBS simulation would take effect. The spikes have burst oscillations with DBS, and when the DBS effect ends, there are 14 spikes to maintain the healthy state until the disease begins. It should be noted that the DBS has been used for a long time in the temporal model for the present study. These findings are accurate and have been validated by the previous studies for the discrete brain network model. The developed neuronal model and the results presented in this study provide an important initial step not only for our better understanding of the cortex–BGTH brain network dynamics in healthy and PD states but also pave the way for the generation of new models for optimizing and designing discrete brain networks assisting in the development of brain pathologies. Moreover, the co-simulation model presented here can be used to personalize deep brain stimulation for specific patients. Since it is unethical to directly experiment on the transmission of neurodegenerative disease among humans, stochastic models of the spread of diseases such as PD are an essential tool for analyzing and quantifying the dynamics of propagation. The integration of stochastic modeling techniques allowing to handle additional coupled dynamic effects that are increasingly important in the PD analysis [98] can further enhance the methodology presented here. Future studies will be focused on the inclusion of other brain regions on a large scale and stochastic terms in the presence of white noise.

Declaration of competing interest

The authors declare that they have no known competing financial interests or personal relationships that could have appeared to influence the work reported in this paper.

Data availability

No data was used for the research described in the article.

Acknowledgments

The authors are grateful to the NSERC and the CRC Program for their support. This research was enabled in part by support provided by SHARCNET (www.sharcnet.ca) and Digital Research Alliance of Canada (www.alliancecan.ca).

References

[1] J.O. Dostrovsky, A.M. Lozano, Mechanisms of deep brain stimulation, Mov. Disorders: Offic. J. Mov. Disord. Soc. 17 (S3) (2002) S63–S68.

[2] J.L. Plotkin, J.A. Goldberg, Thinking outside the box (and arrow): current themes in striatal dysfunction in movement disorders, The Neuroscientist 25 (4) (2019) 359–379.

[3] B. Hollunder, N. Rajamani, S.H. Siddiqi, C. Finke, A.A. Kühn, H.S. Mayberg, M.D. Fox, C. Neudorfer, A. Horn, Toward personalized medicine in connectomic deep brain stimulation, 2021, arXiv preprint arXiv:2109.12327.

[4] K. Ahmad, M.H. Baig, G.K. Gupta, M. Kamal, N. Pathak, I. Choi, Identification of common therapeutic targets for selected neurodegenerative disorders: An in silico approach, J. Comput. Sci. 17 (2016) 292–306.

[5] H. Schroll, F.H. Hamker, Computational models of basal-ganglia pathway functions: focus on functional neuroanatomy, Front. Syst. Neurosci. 7 (2013) 122.

[6] Y. Cakir, Computational neuronal correlation with enhanced synchronized activity in the basal ganglia and the slowing of thalamic theta and alpha rhythms in Parkinson's disease, Eur. J. Neurosci. 54 (3) (2021) 5203–5223.

[7] M. Delong, A. Georgopoulos, M. Crutcher, S. Mitchell, R. Richardson, G. Alexander, Functional organization of the basal ganglia: contributions of single-cell recording studies, in: Ciba Foundation Symposium, 107, 1984, pp. 64–82.

[8] J.L. Lanciego, N. Luquin, J.A. Obeso, Functional neuroanatomy of the basal ganglia, Cold Spring Harbor Perspectives in Med. 2 (12) (2012) a009621.

[9] H. Shaheen, R. Melnik, Deep brain stimulation with a computational model for the cortex-thalamus-basal-ganglia system and network dynamics of neurological disorders, Comput. Math. Methods 2022 (Article ID 8998150) (2022).

[10] J.K. Wong, E.H. Middlebrooks, S.S. Grewal, L. Almeida, C.W. Hess, M.S. Okun, A comprehensive review of brain connectomics and imaging to improve deep brain stimulation outcomes, Mov. Disorders 35 (5) (2020) 741–751.

[11] T. Tsuboi, M. Charbel, D.T. Peterside, M. Rana, A. Elkouzi, W. Deeb, A. Ramirez-Zamora, J. Lemos Melo Lobo Jofili Lopes, L. Almeida, P.R. Zeilman, et al., Pallidal connectivity profiling of stimulation-induced dyskinesia in Parkinson's disease, Mov. Disorders 36 (2) (2021) 380–388.

[12] M. Lu, X. Wei, Y. Che, J. Wang, K.A. Loparo, Erratum: Application of reinforcement learning to deep brain stimulation in a computational model of Parkinson's disease (IEEE Transactions on Neural Systems and Rehabilitation Engineering (2020) 28: 1 (339–349, IEEE Trans. Neural Syst. Rehabil. Eng. 28 (3) (2020) 766.

[13] J. Zhang, J. Li, F. Chen, X. Liu, C. Jiang, X. Hu, L. Ma, Z. Xu, STN versus GPi deep brain stimulation for dyskinesia improvement in advanced Parkinson's disease: a meta-analysis of randomized controlled trials, Clin. Neurol. Neurosurg. 201 (2021) 106450.

[14] T.M. Herrington, J.J. Cheng, E.N. Eskandar, Mechanisms of deep brain stimulation, J. Neurophysiol. 115 (1) (2016) 19–38.

[15] Y. Yu, X. Wang, Q. Wang, Q. Wang, A review of computational modeling and deep brain stimulation: applications to Parkinson's disease, Appl. Math. Mech. (2020) 1–22.

[16] A.M. Lozano, N. Lipsman, H. Bergman, P. Brown, S. Chabardes, J.W. Chang, K. Matthews, C.C. McIntyre, T.E. Schlaepfer, M. Schulder, et al., Deep brain stimulation: current challenges and future directions, Nat. Rev. Neurol. 15 (3) (2019) 148–160.

[17] J. Baladron, A. Nambu, F.H. Hamker, The subthalamic nucleus-external globus pallidus loop biases exploratory decisions towards known alternatives: a neuro-computational study, Eur. J. Neurosci. 49 (6) (2019) 754–767.

[18] O. Maith, F. Villagrasa Escudero, H.Ü. Dinkelbach, J. Baladron, A. Horn, F. Irmen, A.A. Kühn, F.H. Hamker, A computational model-based analysis of basal ganglia pathway changes in Parkinson's disease inferred from resting-state fMRI, Eur. J. Neurosci. 53 (7) (2021) 2278–2295.

[19] J.E. Rubin, D. Terman, High frequency stimulation of the subthalamic nucleus eliminates pathological thalamic rhythmicity in a computational model, J. Comput. Neurosci. 16 (3) (2004) 211–235.

[20] G. Halnes, T. Mäki-Marttunen, D. Keller, K.H. Pettersen, O.A. Andreassen, G.T. Einevoll, Effect of ionic diffusion on extracellular potentials in neural tissue, PLoS Comput. Biol. 12 (11) (2016) e1005193.

[21] S. Jin, Z. Zador, A. Verkman, Random-walk model of diffusion in three dimensions in brain extracellular space: comparison with microfiberoptic photobleaching measurements, Biophys. J. 95 (4) (2008) 1785–1794.

[22] E. Syková, Diffusion properties of the brain in health and disease, Neurochem. Int. 45 (4) (2004) 453–466.

[23] E. Syková, C. Nicholson, Diffusion in brain extracellular space, Physiol. Rev. 88 (4) (2008) 1277–1340.

[24] J.J. Ackerman, J.J. Neil, The use of MR-detectable reporter molecules and ions to evaluate diffusion in normal and ischemic brain, NMR Biomed. 23 (7) (2010) 725–733.

[25] B. Jeurissen, M. Descoteaux, S. Mori, A. Leemans, Diffusion MRI fiber tractography of the brain, NMR Biomed. 32 (4) (2019) e3785.

[26] E. Solomon, G. Liberman, Z. Zhang, L. Frydman, Diffusion MRI measurements in challenging head and brain regions via cross-term spatiotemporally encoding, Sci. Rep. 7 (1) (2017) 1–10.

[27] C. Kelley, A.J. Newton, S. Hrabetova, R.A. McDougal, W.W. Lytton, Multiscale computer modeling of spreading depolarization in brain slices, 2022, BioRxiv.

[28] R.G. Thorne, S. Hrabetová, C. Nicholson, Diffusion of epidermal growth factor in rat brain extracellular space measured by integrative optical imaging, J. Neurophysiol. 92 (6) (2004) 3471–3481.

[29] S.K. Tan, R. Vlamings, L. Lim, T. Sesia, M.L. Janssen, H.W. Steinbusch, V. Visser-Vandewalle, Y. Temel, Experimental deep brain stimulation in animal models, Neurosurgery 67 (4) (2010) 1073–1080.

[30] P. Gubellini, P. Salin, L. Kerkerian-Le Goff, C. Baunez, Deep brain stimulation in neurological diseases and experimental models: from molecule to complex behavior, Prog. Neurobiol. 89 (1) (2009) 79–123.

[31] S. Knorr, T. Musacchio, R. Paulat, C. Matthies, H. Endres, N. Wenger, C. Harms, C.W. Ip, Experimental deep brain stimulation in rodent models of movement disorders, Exp. Neurol. 348 (2022) 113926.

[32] R. Enger, W. Tang, G.F. Vindedal, V. Jensen, P. Johannes Helm, R. Sprengel, L.L. Looger, E.A. Nagelhus, Dynamics of ionic shifts in cortical spreading depression, Cerebral Cortex 25 (11) (2015) 4469–4476.

[33] G. Buzsáki, C.A. Anastassiou, C. Koch, The origin of extracellular fields and currents—EEG, ECoG, LFP and spikes, Nat. Rev. Neurosci. 13 (6) (2012) 407–420.

[34] T.B. Thompson, P. Chaggar, E. Kuhl, A. Goriely, Alzheimer's Disease Neuroimaging Initiative, Protein-protein interactions in neurodegenerative diseases: a conspiracy theory, PLoS Comput. Biol. 16 (10) (2020) e1008267.

[35] G.C. Peng, M. Alber, A.B. Tepole, W.R. Cannon, S. De, S. Dura-Bernal, K. Garikipati, G. Karniadakis, W.W. Lytton, P. Perdikaris, et al., Multiscale modeling meets machine learning: What can we learn? Arch. Comput. Methods Eng. 28 (3) (2021) 1017–1037.

[36] S. Pal, R. Melnik, Nonlocal models in the analysis of brain neurodegenerative protein dynamics with application to alzheimer's disease, Sci. Rep. 12 (1) (2022) 1–13.

[37] J.M. Meier, D. Perdikis, A. Blickensdörfer, L. Stefanovski, Q. Liu, O. Maith, H.Ü. Dinkelbach, J. Baladron, F.H. Hamker, P. Ritter, Virtual deep brain stimulation: Multiscale co-simulation of a spiking basal ganglia model and a whole-brain mean-field model with the virtual brain, Exp. Neurol. (2022) 114111.

[38] M. Schirner, A.R. McIntosh, V. Jirsa, G. Deco, P. Ritter, Inferring multi-scale neural mechanisms with brain network modelling, Elife 7 (2018) e28927.

[39] B. Tadić, R. Melnik, Self-organised critical dynamics as a key to fundamental features of complexity in physical, biological, and social networks, Dynamics 1 (2) (2021) 181–197.

[40] P. Sanz-Leon, S.A. Knock, A. Spiegler, V.K. Jirsa, Mathematical framework for large-scale brain network modeling in the Virtual Brain, Neuroimage 111 (2015) 385–430.

[41] M. Kujdowicz, D. Adamek, The diffusion weighted imaging of the brain stroke–what Lies beneath 'diffusion', Clin. Image Case Rep J. 4 (9) (2022) 258, www.literaturepublishers.org.

[42] T. Jin, S.-G. Kim, Functional changes of apparent diffusion coefficient during visual stimulation investigated by diffusion-weighted gradient-echo fMRI, Neuroimage 41 (3) (2008) 801–812.

[43] A. Darquié, J.-B. Poline, C. Poupon, H. Saint-Jalmes, D. Le Bihan, Transient decrease in water diffusion observed in human occipital cortex during visual stimulation, Proc. Natl. Acad. Sci. 98 (16) (2001) 9391–9395.

[44] Y. Komaki, C. Debacker, B. Djemai, L. Ciobanu, T. Tsurugizawa, D.L. Bihan, Differential effects of aquaporin-4 channel inhibition on BOLD fMRI and diffusion fMRI responses in mouse visual cortex, Plos One 15 (5) (2020) e0228759.

[45] R. Casero, U. Siedlecka, E.S. Jones, L. Gruscheski, M. Gibb, J.E. Schneider, P. Kohl, V. Grau, Transformation diffusion reconstruction of three-dimensional histology volumes from two-dimensional image stacks, Med. Image Anal. 38 (2017) 184–204.

[46] J. Sepulcre, H. Liu, T. Talukdar, I. Martincorena, B.T. Yeo, R.L. Buckner, The organization of local and distant functional connectivity in the human brain, PLoS Comput. Biol. 6 (6) (2010) e1000808.

[47] A. Andree, N. Li, K. Butenko, M. Kober, J.Z. Chen, T. Higuchi, M. Fauser, A. Storch, C.W. Ip, A.A. Kühn, et al., Deep brain stimulation electrode modeling in rats, Exp. Neurol. 350 (2022) 113978.

[48] R. Li, C. Zhang, Y. Rao, T.-F. Yuan, Deep brain stimulation of fornix for memory improvement in Alzheimer's disease: A critical review, Ageing Res. Rev. (2022) 101668.

[49] J. Peeters, A. Boogers, T. Van Bogaert, H. Davidoff, R. Gransier, J. Wouters, B. Nuttin, M. Mc Laughlin, Electrophysiologic evidence that directional deep brain stimulation activates distinct neural circuits in patients with Parkinson disease, Neuromodulation: Technology At the Neural Interface (2022).

[50] S. Atasoy, I. Donnelly, J. Pearson, Human brain networks function in connectome-specific harmonic waves, Nature Commun. 7 (1) (2016) 1–10.

[51] X. Liu, C. Ren, Z. Huang, M. Wilson, J.-H. Kim, Y. Lu, M. Ramezani, T. Komiyama, D. Kuzum, Decoding of cortex-wide brain activity from local recordings of neural potentials, J. Neural Eng. 18 (6) (2021) 066009.

[52] K. Kumaravelu, D.T. Brocker, W.M. Grill, A biophysical model of the cortex-basal ganglia-thalamus network in the 6-OHDA lesioned rat model of Parkinson's disease, J. Comput. Neurosci. 40 (2) (2016) 207–229.

[53] R.Q. So, A.R. Kent, W.M. Grill, Relative contributions of local cell and passing fiber activation and silencing to changes in thalamic fidelity during deep brain stimulation and lesioning: a computational modeling study, J. Comput. Neurosci. 32 (3) (2012) 499–519.
[54] P.C. Bressloff, Waves in neural media, Lect. Notes Math. Modell. Life Sci. (2014) 18–19.
[55] F. Matthäus, A comparison of modeling approaches for the spread of prion diseases in the brain, in: Modelling Dynamics in Processes and Systems, Springer, 2009, pp. 109–117.
[56] F. Matthaeus, The spread of prion diseases in the brain-models of reaction and transport on networks, J. Biol. Systems 17 (04) (2009) 623–641.
[57] J.A. McNab, B.L. Edlow, T. Witzel, S.Y. Huang, H. Bhat, K. Heberlein, T. Feiweier, K. Liu, B. Keil, J. Cohen-Adad, et al., The human connectome project and beyond: initial applications of 300 mT/m gradients, Neuroimage 80 (2013) 234–245.
[58] B. Szalkai, C. Kerepesi, B. Varga, V. Grolmusz, Parameterizable consensus connectomes from the human connectome project: The budapest reference connectome server v3. 0, Cogn. Neurodyn. 11 (1) (2017) 113–116.
[59] C. Kerepesi, B. Szalkai, B. Varga, V. Grolmusz, How to direct the edges of the connectomes: Dynamics of the consensus connectomes and the development of the connections in the human brain, Plos One 11 (6) (2016) e0158680.
[60] F. Irmen, A. Horn, D. Meder, W.-J. Neumann, P. Plettig, G.-H. Schneider, H.R. Siebner, A.A. Kühn, Sensorimotor subthalamic stimulation restores risk-reward trade-off in Parkinson's disease, Mov. Disorders 34 (3) (2019) 366–376.
[61] Y. Zhang, M.A. Burock, Diffusion tensor imaging in Parkinson's disease and parkinsonian syndrome: a systematic review, Front. Neurol. 11 (2020) 1091.
[62] V.M. Saenger, J. Kahan, T. Foltynie, K. Friston, T.Z. Aziz, A.L. Green, T.J. van Hartevelt, J. Cabral, A.B. Stevner, H.M. Fernandes, et al., Uncovering the underlying mechanisms and whole-brain dynamics of deep brain stimulation for Parkinson's disease, Sci. Rep. 7 (1) (2017) 1–14.
[63] Q. Fang, Y.-t. Li, B. Peng, Z. Li, L.I. Zhang, H.W. Tao, Balanced enhancements of synaptic excitation and inhibition underlie developmental maturation of receptive fields in the mouse visual cortex, J. Neurosci. 41 (49) (2021) 10065–10079.
[64] L.Y. Prince, T. Bacon, R. Humphries, K. Tsaneva-Atanasova, C. Clopath, J.R. Mellor, Separable actions of acetylcholine and noradrenaline on neuronal ensemble formation in hippocampal CA3 circuits, PLoS Comput. Biol. 17 (10) (2021) e1009435.
[65] A. Donato, K. Kagias, Y. Zhang, M.A. Hilliard, Neuronal subcompartmentalization: a strategy to optimize neuronal function, Biol. Rev. 94 (3) (2019) 1023–1037.
[66] J.P. Bolam, E.K. Pissadaki, Living on the edge with too many mouths to feed: why dopamine neurons die, Mov. Disorders 27 (12) (2012) 1478–1483.
[67] D.J. Surmeier, J.A. Obeso, G.M. Halliday, Selective neuronal vulnerability in Parkinson disease, Nat. Rev. Neurosci. 18 (2) (2017) 101–113.
[68] M. Mamelak, Parkinson's disease, the dopaminergic neuron and gammahydroxybutyrate, Neurol. Ther. 7 (1) (2018) 5–11.
[69] Y. Guo, J.E. Rubin, C.C. McIntyre, J.L. Vitek, D. Terman, Thalamocortical relay fidelity varies across subthalamic nucleus deep brain stimulation protocols in a data-driven computational model, J. Neurophysiol. 99 (3) (2008) 1477–1492.
[70] A.D. Dorval, A.M. Kuncel, M.J. Birdno, D.A. Turner, W.M. Grill, Deep brain stimulation alleviates parkinsonian bradykinesia by regularizing pallidal activity, J. Neurophysiol. 104 (2) (2010) 911–921.
[71] M. Fauser, M. Ricken, F. Markert, N. Weis, O. Schmitt, J. Gimsa, C. Winter, K. Badstübner-Meeske, A. Storch, Subthalamic nucleus deep brain stimulation induces sustained neurorestoration in the mesolimbic dopaminergic system in a Parkinson's disease model, Neurobiol. Dis. (2021) 105404.
[72] M. Jahanshahi, Effects of deep brain stimulation of the subthalamic nucleus on inhibitory and executive control over prepotent responses in Parkinson's disease, Front. Syst. Neurosci. 7 (2013) 118.
[73] J. Herzog, B. Möller, K. Witt, M.O. Pinsker, G. Deuschl, J. Volkmann, Influence of subthalamic deep brain stimulation versus levodopa on motor perseverations in Parkinson's disease, Mov. Disorders 24 (8) (2009) 1206–1210.
[74] L. Goenner, O. Maith, I. Koulouri, J. Baladron, F.H. Hamker, A spiking model of basal ganglia dynamics in stopping behavior supported by arkypallidal neurons, Eur. J. Neurosci. 53 (7) (2021) 2296–2321.
[75] C. Martinez-Gonzalez, J.P. Bolam, J. Mena-Segovia, Topographical organization of the pedunculopontine nucleus, Front. Neuroanat. 5 (2011) 22.
[76] A. Le Pogam, M. Hatt, P. Descourt, N. Boussion, C. Tsoumpas, F.E. Turkheimer, C. Prunier-Aesch, J.-L. Baulieu, D. Guilloteau, D. Visvikis, Evaluation of a 3D local multiresolution algorithm for the correction of partial volume effects in positron emission tomography, Med. Phys. 38 (9) (2011) 4920–4933.
[77] M. Sedrak, A. Gorgulho, A. Frew, E. Behnke, A. DeSalles, N. Pouratian, Diffusion tensor imaging and colored fractional anisotropy mapping of the ventralis intermedius nucleus of the thalamus, Neurosurgery 69 (5) (2011) 1124–1130.
[78] E.A. Disbrow, N.D. Glassy, E.M. Dressler, K. Russo, E.A. Franz, R.S. Turner, M.I. Ventura, L. Hinkley, R. Zweig, S.S. Nagarajan, et al., Cortical oscillatory dysfunction in Parkinson disease during movement activation and inhibition, PLoS One 17 (3) (2022) e0257711.
[79] N. Vanegas-Arroyave, P.M. Lauro, L. Huang, M. Hallett, S.G. Horovitz, K.A. Zaghloul, C. Lungu, Tractography patterns of subthalamic nucleus deep brain stimulation, Brain 139 (4) (2016) 1200–1210.
[80] D. Milardi, A. Quartarone, A. Bramanti, G. Anastasi, S. Bertino, G.A. Basile, P. Buonasera, G. Pilone, G. Celeste, G. Rizzo, et al., The cortico-basal ganglia-cerebellar network: past, present and future perspectives, Front. Syst. Neurosci. 13 (2019) 61.
[81] P. Perdikaris, L. Grinberg, G.E. Karniadakis, Multiscale modeling and simulation of brain blood flow, Phys. Fluids 28 (2) (2016) 021304.
[82] M.V. Petersen, J. Mlakar, S.N. Haber, M. Parent, Y. Smith, P.L. Strick, M.A. Griswold, C.C. McIntyre, Holographic reconstruction of axonal pathways in the human brain, Neuron 104 (6) (2019) 1056–1064.
[83] Q. Wang, H. Akram, M. Muthuraman, G. Gonzalez-Escamilla, S.A. Sheth, S. Oxenford, F.-C. Yeh, S. Groppa, N. Vanegas-Arroyave, L. Zrinzo, et al., Normative vs. patient-specific brain connectivity in deep brain stimulation, Neuroimage 224 (2021) 117307.
[84] E.H. Middlebrooks, I. Tuna, S. Grewal, L. Almeida, M. Heckman, E. Lesser, K. Foote, M. Okun, V. Holanda, Segmentation of the globus pallidus internus using probabilistic diffusion tractography for deep brain stimulation targeting in Parkinson disease, Am. J. Neuroradiol. 39 (6) (2018) 1127–1134.
[85] R. Fuchs, H. Hauser, Visualization of multi-variate scientific data, in: Computer Graphics Forum, 28, (6) Wiley Online Library, 2009, pp. 1670–1690.
[86] R. Colbourn, A. Naik, S. Hrabetova, ECS dynamism and its influence on neuronal excitability and seizures, Neuroche. Res. 44 (5) (2019) 1020–1036.
[87] L.F. Agnati, M. Marcoli, G. Maura, A. Woods, D. Guidolin, The brain as a "hyper-network": the key role of neural networks as main producers of the integrated brain actions especially via the "broadcasted" neuroconnectomics, J. Neural Transm. 125 (6) (2018) 883–897.
[88] P. Kamali-Zare, C. Nicholson, Brain extracellular space: geometry, matrix and physiological importance, Basic Clin. Neurosci. 4 (4) (2013) 282.
[89] D.J. Wolak, R.G. Thorne, Diffusion of macromolecules in the brain: implications for drug delivery, Mol. Pharma. 10 (5) (2013) 1492–1504.
[90] A.D. Dorval, G.S. Russo, T. Hashimoto, W. Xu, W.M. Grill, J.L. Vitek, Deep brain stimulation reduces neuronal entropy in the MPTP-primate model of Parkinson's disease, J. Neurophysiol. 100 (5) (2008) 2807–2818.
[91] M. Filali, W.D. Hutchison, V.N. Palter, A.M. Lozano, J.O. Dostrovsky, Stimulation-induced inhibition of neuronal firing in human subthalamic nucleus, Exp. Brain Res. 156 (3) (2004) 274–281.
[92] M.-L. Welter, P. Burbaud, S. Fernandez-Vidal, E. Bardinet, J. Coste, B. Piallat, M. Borg, S. Besnard, P. Sauleau, B. Devaux, et al., Basal ganglia dysfunction in OCD: subthalamic neuronal activity correlates with symptoms severity and predicts high-frequency stimulation efficacy, Translational Psychiatry 1 (5) (2011) e5.
[93] D. Milardi, A. Arrigo, G. Anastasi, A. Cacciola, S. Marino, E. Mormina, A. Calamuneri, D. Bruschetta, G. Cutroneo, F. Trimarchi, et al., Extensive direct subcortical cerebellum-basal ganglia connections in human brain as revealed by constrained spherical deconvolution tractography, Front. Neuroanat. 10 (2016) 29.
[94] A. Arrigo, A. Calamuneri, D. Milardi, E. Mormina, M. Gaeta, F. Corallo, V.L. Buono, G. Chillemi, S. Marino, A. Cacciola, et al., Claustral structural connectivity and cognitive impairment in drug naïve Parkinson's disease, Brain Imaging and Behavior 13 (4) (2019) 933–944.
[95] R.J. Theilmann, J.D. Reed, D.D. Song, M.X. Huang, R.R. Lee, I. Litvan, D.L. Harrington, White-matter changes correlate with cognitive functioning in Parkinson's disease, Front. Neurol. 4 (2013) 37.
[96] H. Fan, Z. Zheng, Z. Yin, J. Zhang, G. Lu, Deep brain stimulation treating dystonia: A systematic review of targets, body distributions and etiology classifications, Front. Hum. Neurosci. 15 (2021).
[97] Y.-S. Chen, M.-H. Chen, C.-H. Lu, P.-C. Chen, H.-L. Chen, I. Yang, N.-W. Tsai, W.-C. Lin, et al., Associations among cognitive functions, plasma DNA, and white matter integrity in patients with early-onset Parkinson's disease, Front. Neurosci. 11 (2017) 9.
[98] T.K.T. Thieu, R. Melnik, Coupled effects of channels and synaptic dynamics in stochastic modelling of healthy and Parkinson's-disease-affected brains, AIMS Bioeng. 9 (2) (2022) 213–238.